Physics – Uspekhi **56** (1) 49 – 78 (2013)

REVIEWS OF TOPICAL PROBLEMS PACS numbers: **47.11. – j**, **47.27. – i**, 47.27.ek, 52.25.Dg

Nonequilibrium Kolmogorov-type particle distributions and their applications

V E Zakharov, V I Karas'

DOI: 10.3367/UFNe.0183.201301c.0055

Contents

Abstract. The paper reviews the current state of research on nonequilibrium (Kolmogorov type) stationary and nonstationary distributions of particles with statically screened Coulomb interaction that are exact solutions of the Boltzmann or Landau collision integral with a source and a sink ensuring the energy flow along the spectrum in momentum space. Analysis is made of the advantages of the new process (based on nonequilibrium distributions) of energy conversion and of the time-dependent nonequilibrium kinetics of an electron–phonon system of a crystal in a strong electric field (electroplastic effect).

V E Zakharov Lebedev Physical Institute,
Russian Academy of Sciences,
Leninskii prosp. 53, 119991 Moscow, Russian Federation,
L D Landau Institute for Theoretical Physics,
Russian Academy of Sciences,
142432 Chernogolovka, Moscow region, Russian Federation
Tel. +7 (499) 132 67 51
E-mail: zakharov@itp.ac.ru
V I Karas' National Scientific Center
'Kharkov Institute of Physics and Technology',
National Academy of Sciences of Ukraine,
ul. Akademicheskaya 1, 61108 Kharkov, Ukraine
Tel. +38 (057) 700 11 46. Fax +38 (057) 335 35 64
E-mail: karas@kipt.kharkov.ua

Received 23 December 2011
Uspekhi Fizicheskikh Nauk **183** (1) 55 – 85 (2013)
DOI: 10.3367/UFNr.0183.201301c.0055
Translated by S D Danilov; edited by A Radzig

1. Introduction

Interest in the nonequilibrium states of various physical systems is steadily growing at present, motivated by the development and extensive use of powerful particle and energy sources.

A universal (independent of the structure of a source and a sink) nonequilibrium stationary energy distribution over wavenumbers ε_k was first proposed by A N Kolmogoroff [1] in the theory of turbulence in an incompressible fluid for the interval of scales $2\pi/k$ intermediate between the scales of forced and efficiently damped motions. The well-known Kolmogorov spectrum of hydrodynamical turbulence has the form

$$\varepsilon_k = AP_1^{2/3}k^{-11/3}\,, \tag{1.1}$$

where A is a constant, P_1 is the spectral energy flux, and k is the wavenumber.

The derivation of formula (1.1) relies on the locality hypothesis in the turbulent motion, i.e., only comparable motion scales significantly interact with each other. This hypothesis remains unproven for the turbulence in an incompressible fluid (strong turbulence, etc.).

In physical systems allowing a description of the interaction between waves or particles in terms of the kinetic equations for waves, quasiparticles, or particles, the derivation of nonequilibrium stationary distributions reduces to solving kinetic equations. In this case, the locality of nonequilibrium stationary distribution corresponds to the convergence of the collision integral. Universal wave spectra that are solutions of the wave collision integral were first found by V E Zakharov [2] in the framework of the theory of weak turbulence of waves.

2. Theoretical studies of nonequilibrium stationary particle distribution functions with flux over spectrum

The Fermi–Dirac or Maxwell distribution function, representing the exact solutions of the respective quantum or classical Boltzmann collision integral, are the thermodynamically equilibrium distribution functions for electrons in degenerate or classical plasmas in the isotropic and spatially homogeneous case [3–7]. For a classical (nondegenerate) gas, the kinetic Boltzmann equation is written down as

$$\frac{\partial f(\mathbf{p})}{\partial t} = \int \mathrm{d}\mathbf{p}_1\,\mathrm{d}\mathbf{p}_2\,\mathrm{d}\mathbf{p}_3\,W\bigl(\mathbf{p},\mathbf{p}_1|\,\mathbf{p}_2,\mathbf{p}_3\bigr) \times \bigl[f(\mathbf{p}_2)f(\mathbf{p}_3)-f(\mathbf{p})f(\mathbf{p}_1)\bigr] \times \delta(E+E_1-E_2-E_3)\,\delta(\mathbf{p}+\mathbf{p}_1-\mathbf{p}_2-\mathbf{p}_3)\,, \quad (2.1)$$

where $W\bigl(\mathbf{p},\mathbf{p}_1|\,\mathbf{p}_2,\mathbf{p}_3\bigr)$ is the transition probability due to collisions, $f(\mathbf{p})$ is the electron distribution function, $\mathbf{p}_l$ and E_l are the momentum and energy of an lth electron, and $\delta(x)$ is the Dirac delta function.

A distribution function which satisfies the condition

$$f(\mathbf{p}_2)f(\mathbf{p}_3)-f(\mathbf{p})f(\mathbf{p}_1)=0 \quad (2.2)$$

is a stationary solution to equation (2.1).

It can readily be seen that functional equation (2.2), with account for energy and momentum conservation laws in particle collisions, leads to the thermodynamically equilibrium Maxwell distribution function.

The question concerning a nonequilibrium distribution function for a small portion of electrons that are relaxing on the equilibrium 'background' (the collision integral allows linearization in this case) in the presence of a uniform energy flux I_1 in momentum space, driven by ionization and recombination processes, has been addressed earlier (see, for example, monograph [8]). Closely related questions on the distribution function for neutrons in crystals were considered by A I Akhiezer and I Ya Pomeranchuk [9]. In these cases, the distribution function may noticeably deviate from the thermodynamically equilibrium solution, while its form turns out to be dependent on the structure of a source and a sink.

Universal nonequilibrium stationary power-law particle distributions ($f=Ap^{2s}$), which are exact solutions of the Boltzmann collision integral, were first obtained by A V Kats, V M Kontorovich, V E Novikov, and S S Moiseev [10, 11] by the group symmetry method. For such distributions to form, the source and sink of particles or energy must exist in momentum space, thus maintaining a constant spectral flux.

In order to determine the power-law exponent s for the transition probability, which is a homogeneous function of momenta of degree n, it is natural to use $\mathbf{p}_l/p$ variables in the integrand. In this case, equation (2.1) reduces to an integral that does not depend on p and the factor p^{4s+n+4}. Let us determine the particle (I_0) and energy (I_1) fluxes in momentum space. The fluxes are linked to the collision integral in the following way:

$$\mathrm{div}\left(j_i(p)\,\frac{\mathbf{p}}{p}\right) = -E^i\left(\frac{\partial f}{\partial t}\right)_{\mathrm{st}}, \quad (2.3)$$

where $I_i=4\pi p^2 j_i$, and E is the particle energy. Solving equation (2.3) yields

$$I_i = A^2\alpha^{1-i}\,\frac{R(s,n)}{4s+n+9+2(i-1)}\,p^{4s+n+9+2(i-1)}\,, \quad (2.4)$$

where $\alpha=\mathrm{const}$, and n is the homogeneity index of transition probability.

From Eqn (2.4) it follows that for s_i satisfying the condition

$$\gamma_s = 4s_i+n+9+2(i-1)=0\,, \quad i=0,1\,, \quad (2.5)$$

the flux I_i is either constant in momentum space or zero if $R(s,n)$ has a zero of the first order at $s=s_i$ (the collision integral is then equal to zero). The distribution function Ap^{2s} corresponds to a nonequilibrium stationary case with a constant energy or particle flux. In this case, the flux direction is set by the sign of the derivative $\mathrm{d}R/\mathrm{d}\gamma_s$ at $\gamma_s=0$, and A is defined by the expression

$$A^2 = I_i\,\alpha^{i-1}\lim_{\gamma_s\to 0}\left|\frac{\mathrm{d}R}{\mathrm{d}\gamma_s}\right|^{-1}. \quad (2.6)$$

Let us demonstrate through direct computations [12, 13] that for the Boltzmann and Landau collision integrals the function $R(s,n)$ satisfies the conditions formulated above in the case of nonequilibrium power-law distributions.

2.1 Exact solutions for the Landau collision integral

It is well known that in plasmas the collision integral describing the interaction between charged particles can be written in the Landau form (see, for example, book [3]):

$$\left(\frac{\partial f(\mathbf{p})}{\partial t}\right)_{\mathrm{st}} = -\mathrm{div}\,\mathbf{j}_0,\ j_{0i}=\pi e^4\Lambda\int \mathrm{d}\mathbf{p}'\,\frac{u^2\delta_{ik}-u_iu_k}{u^3} \times\left[f(\mathbf{p})\,\frac{\partial f(\mathbf{p}')}{\partial p_k'}-f(\mathbf{p}')\,\frac{\partial f(\mathbf{p})}{\partial p_k}\right], \quad (2.7)$$

where $\mathbf{u}=(\mathbf{p}-\mathbf{p}')/m$, Λ is the Coulomb logarithm, and m and e are the electron mass and charge, respectively. Inserting the isotropic power-law distribution function Ap^{2s} into Eqn (2.7) and performing fairly simple calculations, one arrives at the following expression

$$\left(\frac{\partial f(\mathbf{p})}{\partial t}\right)_{\mathrm{st}} = 16\pi^2 me^4\Lambda A^2 p^{4s}\,\frac{(4s+3)(4s+5)}{(s+1)(2s+3)(2s+5)} + \frac{16\pi^2 me^4\Lambda A^2 p^{4s}}{3}\lim_{\substack{p_1\to 0\\ p_2\to\infty}}\left\{\frac{2s^2}{2s+3}\left(\frac{p_1}{p}\right)^{2s+3} + \frac{(2s+1)\,s}{2s+2}\left(\frac{p_2}{p}\right)^{2s+2} - \frac{2s+3}{2}\left(\frac{p_2}{p}\right)^{2s} - \frac{(2s-2)\,s}{2s+5}\left(\frac{p_1}{p}\right)^{2s+5}\right\}. \quad (2.8)$$

According to expression (2.8), the first term of the collision integral, i.e., the function $R(s,n)$, does indeed contain multipliers $4s+5$ and $4s+3$, and to the first power. This ensures, on the one hand, the constancy of energy flux, and, on the other hand, the disappearance of the collision integral for the power-law exponent $s_1=-5/4$. As concerns the exponent $s_0=-3/4$, it corresponds to a nonlocal distribution function, in which case the collision integral diverges (the second term under the limit sign becomes unbounded).

2.2 Exact solutions for the Boltzmann collision integral

Using expression (2.1) for the Boltzmann collision integral and substituting a power-law particle distribution function in the form Ap^{2s}, with the help of the δ-function expressing the momentum conservation law, we integrate expression (2.1) with respect to $\mathbf{p}_2$. Introducing new variables $\mathbf{p}_1$ and $\mathbf{q}$ instead of $\mathbf{p}_1$ and $\mathbf{p}_3$, we then write down the collision integral in the form

$$\frac{\partial f(\mathbf{p})}{\partial t}=-mA^2\int \mathrm{d}\mathbf{p}_1\,\mathrm{d}\mathbf{q}\,W\bigl(\mathbf{p},\mathbf{p}_1|\,\mathbf{p}+\mathbf{q},\mathbf{p}_1-\mathbf{q}\bigr)\times\left[|\mathbf{p}+\mathbf{q}|^{2s}|\mathbf{p}_1-\mathbf{q}|^{2s}-|p|^{2s}|p_1|^{2s}\right]\delta\bigl(\mathbf{q}(\mathbf{p}_1-\mathbf{p}-\mathbf{q})\bigr)\,, \quad (2.9)$$

where $\mathbf{q}=\mathbf{p}_1-\mathbf{p}_3$. The argument of the δ-function may become zero at $\mathbf{p}_1-\mathbf{p}-\mathbf{q}=0$ or $\mathbf{q}(\mathbf{p}_1-\mathbf{p}-\mathbf{q})=0$. The first case presents no interest, as it simply corresponds to permutation of particles upon their collisions, which sets the expression in square brackets to zero [i.e., it corresponds to condition (2.2)] and, consequently, the condition $(\partial f/\partial t)_{\mathrm{st}}=0$.

Let us introduce the angles θ and θ_1 between the vector $\mathbf{q}$ and vectors $\mathbf{p}$ and $\mathbf{p}_1$, respectively. Changing to spherical coordinates in Eqn (2.9) for $\mathbf{p}_1$ and $\mathbf{q}$, integrating over $\mathbf{p}_1$ with the help of the δ-function, and introducing a dimensionless variable $\tilde{q}$ $(\tilde{q}=q/p)$, we obtain

$$\frac{\partial f(\mathbf{p})}{\partial t}=-mA^2p^{4s+r+4}\int_0^8\tilde{q}\,\mathrm{d}\tilde{q}\int \mathrm{d}O\int \mathrm{d}O_1\tilde{W}\frac{1}{\cos\theta_1}\times\left(\frac{\cos\theta+\tilde{q}}{\cos\theta_1}\right)^2\left\{\left[|1+2\tilde{q}\cos\theta+\tilde{q}^2|^s\right]\times\left|\left(\frac{\cos\theta+\tilde{q}}{\cos\theta_1}\right)^2-2\tilde{q}(\cos\theta+\tilde{q})+\tilde{q}^2\right|^s-\left|\frac{\cos\theta+\tilde{q}}{\cos\theta_1}\right|^{2s}\right\}, \quad (2.10)$$

where r is the dimensionality of the transition probability W, and $\mathrm{d}O_i=\sin\theta_i\,\mathrm{d}\theta_i\,\mathrm{d}\varphi_i$.

Let us determine the particle (I_0) and energy (I_1) fluxes in momentum space, taking into account that in the case under consideration the fluxes can be expressed through the collision integral according to formula (2.3). For the probability W, being a homogeneous function of momenta to power n, $W=C_1q^n$, where C_1 is a constant, and n is any real number (in this case, $n=r$), the collision integral (2.10) can easily be integrated over θ_1, φ, and φ_1 and written down as

$$\left(\frac{\partial f}{\partial t}\right)_{\mathrm{st}}=\frac{2\pi^2mC_1A^2}{s+1}\,p^{4s+n+4}\left[J^{(1)}-J^{(2)}\right],$$

$$J^{(1)}=\int_{-1}^{1}\mathrm{d}x\int_0^\infty \mathrm{d}\tilde{q}\,\tilde{q}^{n+1}|1+2\tilde{q}x+\tilde{q}^2|^s\,|x|^{2s+2}\,,$$

$$J^{(2)}=\int_{-1}^{1}\mathrm{d}x\int_0^\infty \mathrm{d}\tilde{q}\,\tilde{q}^{n+1}|x+\tilde{q}|^{2s+2}\,,\quad x=\cos\theta\,.$$

The integral $J^{(2)}$ can be expressed in terms of beta functions $B(x,y)$ as

$$J^{(2)}=(2s+3)^{-1}\bigl[B(2s+4,n+2)-B(-2s-n-5,2s+4)+B(n+2,-2s-n-5)\bigr]\,.$$

To compute $J^{(1)}$, it is convenient first to carry out integration over $\tilde{q}$ (see, for example, handbook [14]), which gives

$$J^{(1)}=2^{-(2s+1)/2}\,\Gamma\left(\frac{1-2s}{2}\right)B(n+2,-n-2s-2)\times\int_0^1\mathrm{d}x\,x^{2s+2}(1-x^2)^{(2s+1)/4}\bigl[P^{s+1/2}_{n+s+3/2}(-x)+P^{s+1/2}_{n+s+3/2}(x)\bigr]\,,$$

where $P^{\mu}_{\nu}(x)$ is the spherical function. Making use of the property of spherical functions, namely

$$P^{\mu}_{\nu}(-x)=-\frac{\sin(\pi\nu)}{\sin(\pi\mu)}\,P^{\mu}_{\nu}(x)+\frac{\sin\bigl(\pi(\nu+\mu)\bigr)\,\Gamma(\nu+\mu+1)}{\sin(\pi\mu)\,\Gamma(\nu-\mu+1)}\,P^{-\mu}_{\nu}(x)\,,$$

and computing integrals over x, we arrive at

$$J^{(1)}=\frac{B(n+2,-n-2s-2)}{2s+3}\left[\left(1-\frac{\sin\bigl(\pi(s+n+3/2)\bigr)}{\sin\bigl(\pi(s+1/2)\bigr)}\right)\times{}_3F_2\left(\frac{n+2}{2},-\frac{n+2s+2}{2},1;\frac{1-2s}{2},\frac{2s+5}{2};1\right)+\frac{\Gamma(2s+n+3)\,\Gamma(1/2-s)\,\Gamma(s+5/2)\,\Gamma(s+2)}{2^{2s+1}\Gamma(n+2)\,\Gamma\bigl((4s+n+7)/2\bigr)\,\Gamma\bigl((2s-n+3)/2\bigr)}\times\frac{\sin\bigl(\pi(2s+n+2)\bigr)}{\sin\bigl(\pi(s+1/2)\bigr)}\right],$$

where ${}_pF_q(\alpha_1,\ldots,\alpha_p;\beta_1,\ldots,\beta_q;z)$ is the hypergeometric function. Thus, the expression for the function $R(s,n)$ entering into a particular solution for the flux I_i [see formula (2.4)], with account for the expressions obtained earlier for $J^{(1)}$ and $J^{(2)}$, takes the form

$$R(s,n)=\frac{-4\pi^3C_1}{(s+1)(2s+3)}\left\{B(2s+4,\,n+2)-B(-2s-n-5,\,2s+4)+B(n+2,\,-2s-n-5)-\left[B(n+2,\,-n-2s-2)\left(1-\frac{\sin\bigl(\pi(s+n+3/2)\bigr)}{\sin\bigl(\pi(s+1/2)\bigr)}\right)\times{}_3F_2\left(\frac{n+2}{2},-\frac{n+2s+2}{2},1;\frac{1-2s}{2},\frac{2s+5}{2};1\right)+\frac{(4s+n+7)(4s+n+9)\,\pi^2(2s+1)(2s+3)}{2^{2s+5}\Gamma(-2s)\,\Gamma\bigl((4s+n+11)/2\bigr)\,\Gamma\bigl((2s-n+3)/2\bigr)}\times\frac{\Gamma(s+2)}{\sin^2\bigl(\pi(s+1/2)\bigr)}\right]\right\}.$$

In Section 2.1 we considered a quadratic law for particle dispersion. The generalization to an arbitrary dispersion law $E=p^{\varsigma_1}/\alpha_1$ (where α_1 and ς_1 are some constants) does not lead to any principal complications, although the expression for $R(s,n,\varsigma_1)$ may prove to be more cumbersome. As for the power-law exponent s_i in the particle distribution function, it is defined for a general dispersion relation by the following

expression

$$s_i = -\frac{n+9+\varsigma_1(i-1)}{2\varsigma_1}\,. \tag{2.11}$$

It has been found that local nonequilibrium particle distribution functions (the collision integral converges for them) are associated with the power-law exponent s satisfying the conditions

$$-\frac{3}{2} < s_0 < -1\,, \quad -\frac{3}{2} < s_1 < -\frac{5}{4}\,. \tag{2.12}$$

Subscripts 0 (1) stand for $I_0\,(I_1) = \text{const}$.

According to condition (2.5), the following homogeneity indices for the transition probability correspond to the exponents from the ranges (2.12):

$$\begin{aligned} &-3 < n < -1\,, \quad I_0 = \text{const}\,,\\ &-4 < n < -3\,, \quad I_1 = \text{const}\,. \end{aligned} \tag{2.13}$$

2.3 Formation conditions for nonequilibrium stationary particle distribution functions in finite energy intervals

As follows from inequalities (2.13) formulated above, the collision integral diverges (the known singularity of W for small transferred momenta) in the case of the Coulomb interaction ($n = -4$). References [10, 11, 15] propose and Refs [12, 13] show that this divergence is alleviated by Debye screening. Consider the collision integral (2.10); for the transition probability, which corresponds to the screened Coulomb potential $W = 2e^4/(q^2 + a_1^2)^2$ (with q being the transferred momentum, and a_1 the Debye momentum), we get

$$\begin{aligned} \frac{\partial f(\mathbf{p})}{\partial t} = -mA^2 p^{4s} \int_0^\infty \tilde{q}\,\mathrm{d}\tilde{q} \int \mathrm{d}O \int \mathrm{d}O_1\, \frac{2e^4}{(\tilde{q}^2 + a^2)^2}\\ \times \frac{1}{\cos\theta_1}\left(\frac{\cos\theta + \tilde{q}}{\cos\theta_1}\right)^2 \Bigg\{ \left|1 + 2\tilde{q}\cos\theta + \tilde{q}^2\right|^s\\ \times \left| \left(\frac{\cos\theta + \tilde{q}}{\cos\theta_1}\right)^2 - 2\tilde{q}(\cos\theta + \tilde{q}) + \tilde{q}^2 \right|^s\\ - \left|\frac{\cos\theta + \tilde{q}}{\cos\theta_1}\right|^{2s} \Bigg\}, \end{aligned} \tag{2.14}$$

where $\tilde{q} = q/p$, and $a = a_1/p$.

We integrate over the angles θ_1, φ, φ_1, and θ, making use of standard integrals [14], and transform Eqn (2.14) to the sum of two integrals:

$$\begin{aligned} \frac{\partial f(\mathbf{p})}{\partial t} = \frac{-8\pi^2 m e^4 A^2}{(s+1)(2s+3)}\, p^{4s} \Bigg\{ \int_0^1 \frac{\mathrm{d}\tilde{q}\,\tilde{q}}{(\tilde{q}^2 + a^2)^2} \Bigg[(1+\tilde{q}^2)^s\\ \times \left({}_2F_1\left(-s, 2s+3; 2s+4; -\frac{2\tilde{q}}{1+\tilde{q}^2}\right) \right.\\ \left. + {}_2F_1\left(-s, 2s+3; 2s+4; \frac{2\tilde{q}}{1+\tilde{q}^2}\right)\right)\\ - (1+\tilde{q})^{2s+3} - (1-\tilde{q})^{2s+3} \Bigg] + \int_0^1 \frac{\mathrm{d}\tilde{q}\,\tilde{q}^{-2s-2}}{(\tilde{q}^2 a^2 + 1)^2}\\ \times \Bigg[\tilde{q}^3 (1+\tilde{q}^2)^s \left({}_2F_1\left(-s, 2s+3; 2s+4; -\frac{2\tilde{q}}{1+\tilde{q}^2}\right) \right.\\ \left. + {}_2F_1\left(-s, 2s+3; 2s+4; \frac{2\tilde{q}}{1+\tilde{q}^2}\right)\right)\\ - (1+\tilde{q})^{2s+3} + (1-\tilde{q})^{2s+3} \Bigg] \Bigg\}. \end{aligned} \tag{2.15}$$

To find the existence domains for power-law distribution functions which correspond to two different asymptotics of the transition probability W, the collision integral in two limiting cases: $a \ll 1$ and $a \gg 1$ is worth consideration. First, for small values of a ($a \ll 1$), we find the dependence of collision integral (2.15) on a. It can readily be seen that the main contribution in this case comes from the first integral in expression (2.15). Expanding the integrand in powers of $\tilde{q}$ and integrating the resulting series term by term, we obtain the expression for the collision integral:

$$\begin{aligned} \frac{\partial f(\mathbf{p})}{\partial t} = \frac{8\pi^2 m e^4 A^2}{(s+1)(2s+3)}\, p^{4s} \Bigg\{ \frac{(4s+3)(4s+5)}{2s+5} \Bigg[\ln a^2\\ + \frac{(2s+1)(2s+3)(2s+5)\,\pi^2 \Gamma(s+2)}{2^{2s+5}\Gamma(-2s)\,\Gamma((2s+7)/2)\,\Gamma((4s+7)/2)\,\sin^2(\pi(2s+1)/2)} \Bigg]\\ + K_1(s)\, a^2 \ln a^2 + \ldots \Bigg\}. \end{aligned}$$

Computing the energy flux according to formula (2.4), we find that the energy flux is negative and is determined by the logarithmic term only for $a^2 < 0.005$. Within the interval $0.005 < a^2 < 0.1$, the energy flux is directed oppositely (it is positive) to its direction for large momenta.

Thus, it is shown [12, 13] that in the region of momentum space $p \gg a_1$ the Debye screening, first, removes the Coulomb divergence and, second, does not change the exponent of the nonequilibrium stationary particle distribution function for constant energy flux in momentum space. The power-law exponent in this function corresponds to the asymptotics of W with the exponent $n = -4$. Additionally, it is established that within a certain domain in momentum space the direction of energy flux is opposite (positive) to its direction for large momenta. Then there is a local power-law distribution, the particle density in which is determined by the flux intensity. The conservative character of flux is ensured by the source and sink, the positions of which must agree with the flux direction found.

Numerous concrete physical tasks face the question of the formation, under the action of sources and sinks in momentum space, of power-law particle distributions in bounded energy intervals surrounded by domains where the particle distributions are in thermodynamic equilibrium. The electron–electron collision integral in a solid state plasma is computed in the approximation of the quadratic dispersion law. The divergence caused by the Coulomb interaction between particles is removed by the introduction, as above, of a matrix element describing the screened Coulomb interaction. The Boltzmann collision integral in the case of quantum statistics (see, for example, book [3]) can be represented in the form

$$\begin{aligned} \frac{\partial \eta(\mathbf{p})}{\partial t} = \frac{2}{(2\pi\hbar)^6} \int \mathrm{d}\mathbf{p}_1\,\mathrm{d}\mathbf{p}_2\,\mathrm{d}\mathbf{p}_3\, W(\mathbf{p}, \mathbf{p}_1 | \mathbf{p}_2, \mathbf{p}_3)\\ \times \left[\eta(\mathbf{p}_2)\,\eta(\mathbf{p}_3)\big(1-\eta(\mathbf{p})\big)\big(1-\eta(\mathbf{p}_1)\big) - \eta(\mathbf{p})\,\eta(\mathbf{p}_1)\right.\\ \left. \times \big(1-\eta(\mathbf{p}_2)\big)\big(1-\eta(\mathbf{p}_3)\big)\right]\\ \times \delta(E + E_1 - E_2 - E_3)\,\delta(\mathbf{p} + \mathbf{p}_1 - \mathbf{p}_2 - \mathbf{p}_3)\,, \end{aligned} \tag{2.16}$$

where $W = (2\pi\hbar)^3 2e^4 \left(|\mathbf{p}_1 - \mathbf{p}_3|^2 + a_1^2\right)^{-2}$ is the matrix element describing the screened Coulomb interaction, and $\eta(\mathbf{p}_i)$ are the occupation numbers.

Let the electron distribution function be power-law in the inertial range (between the source and sink), and thermo-

dynamically equilibrium (Fermi) outside it, namely

$$\eta_i = \eta_s(\mathbf{p}_i), \text{ if } p' \leqslant |\mathbf{p}_i| \leqslant p'' \left(\eta_s = \frac{(2\pi\hbar)^3}{2}\,\alpha |I_1|^{1/2} p_i^{2s}\right),$$

$$\eta_i = \eta_{\mathrm{F}}(\mathbf{p}_i), \text{ if } p' > |\mathbf{p}_i|, |\mathbf{p}_i| > p'' \left(\eta_{\mathrm{F}} = \left[1 + \exp\frac{p_i^2 - p_{\mathrm{F}}^2}{2mk_{\mathrm{B}}T}\right]^{-1}\right),$$

where α is the proportionality factor, I_1 is the energy flux, p_{F} is the Fermi momentum, k_{B} is the Boltzmann constant, and T is the equilibrium temperature of electron gas. The collision integral is computed with the goal to determine the extent of the inertial range for the power-law distributions η_s; therefore, the momentum p over which there is no integration in Eqn (2.16) should lie in this interval: $\eta = \eta_s(p)$. It has been shown above that the nonequilibrium distribution function may have the form $\eta_s = A_1 p^{2s}$ for metals in the region of momentum space where $a_1 < p$, i.e., the source and sink must be arranged so that the conditions $p', p'' > p_{\mathrm{F}}$ are satisfied. When computing the integral in Eqn (2.16), we will neglect thermal smearing of the Fermi distribution function, because it will only lead to corrections which are insignificant by virtue of the condition $T \ll E_{\mathrm{F}}$ (E_{F} is the Fermi energy). Thus, a step function of unity amplitude can be taken for η_{F}:

$$\eta_{\mathrm{F}} = \theta(p_{\mathrm{F}}^2 - p_i^2)\,,$$

and the unit function is defined hereinafter as

$$\theta(x) = \begin{cases} 0, & x < 0\,, \\ 1, & x \geqslant 0\,. \end{cases}$$

Suppose that $\eta_s \ll 1$ in the entire inertial range. We will evaluate expression (2.16) with an accuracy up to terms logarithmic in a_1, similarly as for the Landau collision integral. This implies that we will account for interactions with a small momentum transfer in collisions. It has been shown above that for power-law distribution functions the nonlogarithmic terms in the Boltzmann collision integral, related to large momentum transfer in collisions, turn out to be important if momenta lie in a certain range characteristic of a solid state plasma in conductors. Computation of nonlogarithmic terms in this case faces considerable difficulties, so the conditions to be derived below take into account only weak momentum exchange and will be valid for the plasma in semiconductors, whereas in the plasma of conductors they are more stringent than necessary. Bearing in mind the remarks and clarifications made above, the collision integral can be represented as

$$\begin{aligned}\frac{\partial\eta(\mathbf{p})}{\partial t} = {} & \frac{2}{(2\pi\hbar)^6}\int_{0\leqslant|p_1|\leqslant p'} \mathrm{d}\mathbf{p}_1\,\mathrm{d}\mathbf{p}_2\,\mathrm{d}\mathbf{p}_3 W \\ & \times \left[\eta_2\eta_3\theta(p_1^2 - p_{\mathrm{F}}^2) - \eta_s\eta_1(1-\eta_2)(1-\eta_3)\right] \\ & \times \delta(E + E_1 - E_2 - E_3)\,\delta(\mathbf{p} + \mathbf{p}_1 - \mathbf{p}_2 - \mathbf{p}_3) \\ & + \frac{2}{(2\pi\hbar)^6}\int_{p'\leqslant|p_1|\leqslant p''} \mathrm{d}\mathbf{p}_1\,\mathrm{d}\mathbf{p}_2\,\mathrm{d}\mathbf{p}_3 W \\ & \times \left[\eta_2\eta_3 - \eta_s\eta_{s1}(1-\eta_2)(1-\eta_3)\right] \\ & \times \delta(E + E_1 - E_2 - E_3)\,\delta(\mathbf{p} + \mathbf{p}_1 - \mathbf{p}_2 - \mathbf{p}_3)\,. \end{aligned} \quad (2.17)$$

We begin with the second integral on the right-hand side of Eqn (2.17), and perform the same manipulations as in the derivation of Eqn (2.10). Integrating over φ and φ_1 and substituting W, which corresponds to the screened Coulomb interaction, we obtain

$$\left(\frac{\partial\eta(p)}{\partial t}\right)_{p'}^{p''} = \int_{0\leqslant(x+q)\,y\leqslant p''} \frac{q\,\mathrm{d}q}{(q^2+a^2)^2}\int \mathrm{d}x \int \mathrm{d}y F(y,x,q) - \int_{0\leqslant(x+q)\,y\leqslant p'} \frac{q\,\mathrm{d}q}{(q^2+a^2)^2}\int \mathrm{d}x \int \mathrm{d}y\, F(y,x,q)\,, \quad (2.18)$$

where

$$F(y,x,q) = \frac{16\pi^2 e^4 m A^2 p^{4s}}{(2\pi\hbar)^3}\,|y|(x+q)^2 \times \left\{(1+2qx+q^2)^s\left[y^2(x+q)^2 - 2qx + q^2\right]^s - |y|^{2s}|x+q|^{2s}\right\},$$

$$q = \frac{|\mathbf{p}_1 - \mathbf{p}_3|}{|\mathbf{p}_1|}\,,\ x = \cos\theta\,,\ y = (\cos\theta_1)^{-1}\,,\ \cos\theta = \frac{|\mathbf{p}\,\mathbf{q}|}{|\mathbf{p}|\,|\mathbf{q}|}\,,$$

$$\cos\theta_1 = \frac{|\mathbf{p}_1\,\mathbf{q}|}{|\mathbf{p}_1||\mathbf{q}|}\,,\ A = \frac{(2\pi\hbar)^3}{2}\,\alpha|I_1|^{1/2}\,.$$

In order to write down the integration limits in Eqn (2.18), one needs to find the domains of existence for the inequalities $0 \leqslant (x+q)\,y \leqslant p''$ and $0 \leqslant (x+q)\,y \leqslant p'$, taking into account that $p'' > 1$, $p' < 1$, $|x| < 1$, and $1 \leqslant |y| < \infty$.

Since the function $F(y,x,q)$ is even with respect to y, after carrying out the change of variable $z = y^2(x+q)^2$, formula (2.18) can be reduced to the form

$$\begin{aligned}\left(\frac{\partial\eta(p)}{\partial t}\right)_{p'}^{p''} = {} & \int_0^{p''-1}\mathrm{d}q\int_{-1}^{1}\mathrm{d}x\int_{(x+q)^2}^{p''^2}\mathrm{d}z\,F_1(z,x,q) \\ & + \int_{p''-1}^{p''+1}\mathrm{d}q\int_{-1}^{p''-q}\mathrm{d}x\int_{(x+q)^2}^{p''^2}\mathrm{d}z\,F_1(z,x,q) \\ & - \int_0^{1-p'}\mathrm{d}q\int_{-p'-q}^{p'-q}\mathrm{d}x\int_{(x+q)^2}^{p'^2}\mathrm{d}z\,F_1(z,x,q) \\ & - \int_{1-p'}^{1+p'}\mathrm{d}q\int_{-1}^{p'-q}\mathrm{d}x\int_{(x+q)^2}^{p'^2}\mathrm{d}z\,F_1(z,x,q)\,, \end{aligned} \quad (2.19)$$

where

$$F_1(z,x,q) = \frac{8\pi^2 e^4 m A^2 p^{4s}}{(2\pi\hbar)^3}\,\frac{q}{(q^2+a^2)^2} \times \left\{(1+2qx+q^2)^s(z-2qx+q^2)^s - z^s\right\}.$$

We will not resolve the behavior of the power-law distribution function near the energy source and sink, i.e., at $p' \approx 1$ and $p'' \approx 1$. Relatedly, to maintain accuracy up to the terms logarithmic in a, it suffices to compute contributions from the first and third terms on the right-hand side of Eqn (2.19). Having performed integration over z and x, we need to expand the integrand in series in q and, since the main contribution comes from $q \leqslant a$, retain only the terms up to those proportional to q^3.

Integration of the first and third terms in Eqn (2.19) results in the following expression

$$\left(\frac{\partial\eta(p)}{\partial t}\right)_{p'}^{p''} = \frac{16\pi^2 e^4 m A^2 p^{4s}}{(2\pi\hbar)^3} \times \left\{\left[\frac{(4s+5)(4s+3)}{(2s+3)(2s+5)(s+1)} + \frac{s(2s+1)}{3(s+1)}\,(p''+1)^{s+1} \times {}_3F_2\left(-s-1, s+\frac{3}{2}, s+1; s+\frac{1}{2}, s; \frac{1}{p''^2+1}\right)\right] \times \int_0^{\min(1,p''-1)} \frac{q^3\,\mathrm{d}q}{(q^2+a^2)^2} + \left[p'^{2s+1} - \frac{2s(-s+1)}{(2s+5)(s+1)} \times p'^{2s+5} - \frac{s(4s+5)}{(2s+3)(s+1)}\,p'^{2s+3} - \frac{2s+3}{3}\,p'^{2s+1}(1+p'^2)^s \times {}_3F_2\left(-s, s+\frac{5}{2}, s+2; s+\frac{3}{2}, s+1; \frac{p'^2}{p''^2+1}\right)\right] \times \int_0^{\min(p', 1-p')} \frac{q^3\,\mathrm{d}q}{(q^2+a^2)^2}\right\}.$$

Let us evaluate the first integral in Eqn (2.17) carrying out the same manipulations as above, with subsequent integration by the formula

$$\int_\alpha^\beta f(x) \prod_{k=1}^n \theta\bigl(\varphi_k(x)\bigr)\,\mathrm{d}x = F(\beta) \prod_{k=1}^n \theta\bigl(\varphi_k(\beta)\bigr) - F(\alpha) \prod_{k=1}^n \theta\bigl(\varphi_k(\alpha)\bigr) - \sum_{l=1}^n \sum_{i=1}^{m_l} F(a_i^l)\,\frac{\varphi_l'(a_i^l)}{|\varphi_l'(a_i^l)|} \times \prod_{\substack{k=1\\k\neq l}}^n \theta\bigl(\varphi_k(a_i^l)\bigr)\bigl[\theta(\beta-a_i^l)\,\theta(a_i^l-\alpha) - \theta(a_i^l-\beta)\,\theta(\alpha-a_i^l)\bigr].$$

The expression for the first integral in Eqn (2.17) will take the form

$$\left(\frac{\partial\eta(p)}{\partial t}\right)_0^{p'} = \frac{32\pi^2 e^4 m A p^{2s}}{(2\pi\hbar)^3}\,p_\mathrm{F}^3\,\frac{s}{3}\int_0^{p'} \frac{q^3\,\mathrm{d}q}{(q^2+a^2)^2}.$$

The final expression for the energy flux in momentum space, which is defined through the collision integral according to relationship (2.3), becomes

$$I_1 = -\frac{32\pi^3 e^4 A^2 p^{4s+5}}{(2\pi\hbar)^3}\left\{\frac{4s+3}{(2s+5)(2s+3)(s+1)} \times \int_0^{\min(1,p''-1)} \frac{q^3\,\mathrm{d}q}{(q^2+a^2)^2} - \frac{s}{3(s+2)}\,p'^{2s+1}\int_0^{p'} \frac{q^3\,\mathrm{d}q}{(q^2+a^2)^2}\right\} - \frac{32\pi^3 e^4 A p^{2s+5}}{(2\pi\hbar)^3}\,\frac{s}{3(2s+5)}\,p_\mathrm{F}^3\int_0^{p'} \frac{q^3\,\mathrm{d}q}{(q^2+a^2)^2}. \tag{2.20}$$

From the last relationship, one can derive a condition to be imposed on the electron density in the vicinity of a sink (the density which governs the source intensity) to keep the flux I_1 constant and, consequently, the distribution η_s close to the universal one in the inertial range (the interval between the source and sink). This condition will be satisfied if the first term in Eqn (2.20) is much larger that the other two:

$$\eta_s(p) \gg p_\mathrm{F}^3\left|\frac{s(2s+3)(s+1)}{3(4s+3)}\right| \int_0^{p''} \frac{q^3\,\mathrm{d}q}{(q^2+a^2)^2} \times \left(\int_0^1 \frac{q^3\,\mathrm{d}q}{(q^2+a^2)^2}\right)^{-1}.$$

Thus, an explicit expression was found for the quantum Boltzmann collision integral as a function of the momentum p, exponent s, momentum p' corresponding to the energy sink, and momentum p'' corresponding to the energy source. It may be concluded that in the absence of particles outside the energy range which is located between the source and sink, the exponent s differs from the universal one by no more than 10% in the limits of the inertial range:

$$|p''-p'| \approx (5-6)\,p_\mathrm{ch}\,, \quad p' \approx p_\mathrm{ch} = 2a_1\,, \tag{2.21a}$$

References [16, 17] consider a case more often encountered in solid state plasmas, where the electron distribution function has a power-law form in the interval between the energy source and sink in momentum space and follows the thermodynamically equilibrium Fermi–Dirac distribution outside it. It is shown that a nonequilibrium stationary distribution of electrons is close to the universal one ($s = -5/4$ for an unbounded inertial range) if the location of source and sink, as well as their intensities, satisfies the conditions specified below. So, the power-law exponent s in the distribution η_s (η_s are the occupation numbers) will differ from $-5/4$ by less than 10% if the following conditions are met:

$$|p''-p'| \approx (5-6)\,p_\mathrm{ch}\,,\ \eta_s(p) \gg 10^{-3}\,,\ p' \approx p_\mathrm{ch} = (2-3)\,a_1. \tag{2.21b}$$

Thus, the nonequilibrium universal electron distribution is possible even if occupation numbers are significantly less (by one or two orders of magnitude) than the equilibrium ones.

3. Theoretical studies of nonequilibrium nonstationary particle distribution functions with flux over spectrum

3.1 Numerical modeling of the formation of particle distribution functions for Landau–Fokker–Planck type equations

3.1.1 Fully conservative difference schemes for Landau–Fokker–Planck type equations. The nonlinear kinetic Boltzmann equation [3–8] describes a system of many particles interacting by the laws of classical mechanics, and serves as the basic equation in models of rarefied gas dynamics. In its general form, the equation for the particle distribution function f_α, depending on spatial coordinates $\mathbf{r}$, velocities $\mathbf{v}$, and time t, can be written down as

$$\frac{\partial f_\alpha}{\partial t} + \mathbf{v}\,\frac{\partial f_\alpha}{\partial \mathbf{r}} + \frac{\mathbf{F}_\alpha}{m_\alpha}\,\frac{\partial f_\alpha}{\partial \mathbf{v}} = \left(\frac{\partial f_\alpha}{\partial t}\right)_\mathrm{st} + S_\alpha\,, \tag{3.1}$$

where m_α is the mass of α particles, F_α is the force acting on an α particle, S_α are the sources (sinks) of particles and energy (open systems), and $(\partial f_\alpha/\partial t)_\mathrm{st}$ is the collision integral. It stands as the fundamental equation in applications requiring a mathematical description of the dynamics of rarefied gases and plasmas. Models of kinetic processes governed by Coulomb collisions occupy a prominent place in applications related to laboratory and magnetospheric plasmas, plasma-chemistry, and solid state plasma.

In plasmas, the Coulomb collisions involving small-angle scattering (with small transferred momentum) are more important than collisions with a substantial change in

velocity (momentum). The collision integral for charged particles was first derived by L D Landau (see, for example, book [3]) from the Boltzmann collision integral, with account for the smallness of momentum transferred in Coulomb collisions and the effect of particle charge screening by other particles outside a sphere with Debye radius. A Landau type equation is also obtained by accounting for small-angle scattering, but for arbitrary potentials of interaction between particles [18–28]. The most pertinent object for modeling with the help of the Landau type collision integral are gases with power-law potentials and an infinite radius of interaction between particles.

The most widely used method of numerical modeling is (regular) finite difference method (Monte Carlo type methods suffer from certain drawbacks for long-range forces). However, a combined approach should be employed, ensuring approximation of equations describing actual dynamics and adequate representation of physical laws underlying the physical model. This approach, based on conservative and fully conservative finite-difference schemes, is related to the work done by A N Tikhonov, A A Samarskii, Yu P Popov, A V Bobylev, I F Potapenko, V A Chuyanov, and others [18–28].

Such an approach, together with high accuracy, gave the capability of obtaining asymptotic solutions in certain cases and testing analytical approaches and other modeling methods.

In a spatially homogeneous case, the Boltzmann collision integral for the distribution function $f(\mathbf{v}, t)$ was written in the form (2.1), where the transition probability W due to collisions is defined by the differential scattering cross section $\sigma(u, \mu)$, which is a function of the relative velocity $u > 0$ and the parameter $\mu = \cos\theta$ ($0 \leqslant \theta \leqslant \pi$ is the scattering angle). Finding the scattering cross section $\sigma(u, \mu)$ for a given interaction potential $U(r)$ is a well-known task in classical mechanics (see, for example, Refs [22–28]).

The collision integral in the Landau form for particles of the same kind carrying the charge e in a spatially-homogeneous case was given in Section 2.1 [see Eqn (2.7)] and may be represented in the form

$$\frac{1}{\Gamma}\left(\frac{\partial f(\mathbf{v})}{\partial t}\right)_{\mathrm{st,\,L}} = \frac{\partial}{\partial v_i}\left\{\int \mathrm{d}\mathbf{w} U_{ij}\left(\frac{\partial}{\partial v_j} - \frac{\partial}{\partial w_j}\right) f(\mathbf{v}) f(\mathbf{w})\right\},$$

$$U_{ij} = \frac{u^2\delta_{ij} - u_i u_j}{u^3}, \qquad (3.2)$$

where $\Gamma = 2\pi e^4 \Lambda / m^2$, and the symmetric kernel U_{ij} is a function of particle relative velocity $\mathbf{u} = \mathbf{v} - \mathbf{w}$. A rough condition for the applicability of equation (3.2) is furnished by the inequality $e^2 n^{1/3} \ll T$, implying that the mean energy of Coulomb interaction is small compared to the mean kinetic energy (n is the particle number density, and T is the temperature expressed in energy units).

3.1.2 Numerical modeling of relaxation of the particle distribution function for the Landau–Fokker–Planck collision integral. Let us consider the relaxation of the initial distribution for gases of particles with power-law interaction potentials in the case of isotropic distribution function $f(\mathbf{v}, t) = f(|\mathbf{v}|, t)$, which obeys the Landau–Fokker–Planck equation in the symmetric form

$$\frac{\partial f}{\partial t} = \frac{1}{v^2}\frac{\partial}{\partial v}\left\{\frac{1}{v}\int_0^\infty \mathrm{d}w\, Q(v, w)\left[wf(w)\frac{\partial f(v)}{\partial v} - vf(v)\frac{\partial f(w)}{\partial w}\right]\right\}, \qquad (3.3)$$

where $Q(v, w)$ is the symmetric kernel, namely

$$Q(v, w) = \frac{\pi}{8} v^3 w^3 \int_{-1}^{1} \mathrm{d}\mu (1 - \mu^2)\, u\sigma(u),$$

$$u^2 = v^2 + w^2 - 2vw\mu.$$

It can be verified that in the absence of sources and sinks the conservation laws for the particle density and energy follow from equation (3.3):

$$n = 4\pi \int_0^\infty \mathrm{d}v\, v^2 f(v, t) = \mathrm{const},$$

$$k_{\mathrm{B}} T = \frac{4\pi m}{3n}\int_0^\infty \mathrm{d}v\, v^4 f(v, t) = \mathrm{const}, \quad t \geqslant 0.$$

The only equilibrium stationary solution to the kinetic Boltzmann equation is furnished by the Maxwell distribution. Exploring the formation of the particle distribution function at energies essentially exceeding the mean energy (the tails of the particle distribution function), apart from its academic interest, can be helpful in tasks related to wave–particle interactions, electron acceleration by a field and tail formation by runaway electrons, and for the problem of thermonuclear fusion (electron cyclotron heating, lower-hybrid resonance, nuclear reactions at the tails of the ion distribution function, and so on). For the Coulomb potential, such research has been conducted in Refs [21–28].

The equilibrium solution takes on the form

$$f_{\mathrm{M}} = \frac{4}{\pi^{1/2}}\left(\frac{3}{2}\right)^{3/2} \exp\left(-\frac{3}{2}v^2\right), \quad v_{\mathrm{th}} = 1,$$

where v_{th} is the thermal velocity. We obtain the conservation laws from equation (3.3) by integrating both its sides over the velocity with an appropriate weight:

$$\frac{\mathrm{d}n}{\mathrm{d}t} = \frac{J}{v}\bigg|_0^\infty = 0, \quad \frac{\mathrm{d}E}{\mathrm{d}t} = (vJ)\big|_0^\infty - 2\int_0^\infty J\,\mathrm{d}v = 0.$$

By applying the integro-differential method to equation (3.3), we obtain the following (implicit) difference scheme:

$$\frac{f_i^k - f_i^{k-1}}{\tau} = \frac{1}{v_i^2 h_{i+1/2}}\left[\frac{J_{i+1/2}^k}{v_{i+1/2}} - \frac{J_{i-1/2}^k}{v_{i-1/2}}\right], \quad i = 2, \ldots, M. \qquad (3.4)$$

The scheme is set forth as the local conservation law for the particle number, whereas the approximation of function J_i must ensure the implementation of energy conservation law. We replace the upper integration limit in Eqn (3.3) by the value of velocity at the last point. Approximating the integrals with the trapezoidal rule, and derivatives with centered differences, yield

$$J_{i+1/2}^k = \sum_{m=1}^{M} Q_{i+1/2,\,m+1/2}\, h_{m+1} \times \left(\frac{f_{i+1}^k - f_i^k}{h_{i+1}}\,\frac{f_m^k v_m + f_{m+1}^k v_{m+1}}{2} - \frac{f_{m+1}^k - f_m^k}{h_{m+1}}\,\frac{f_i^k v_i + f_{i+1}^k v_{i+1}}{2}\right),$$

where $Q_{i+1/2,\,m+1/2} = Q_{m+1/2,\,i+1/2}$. The particle number density is written out as

$$n=\sum_{i=1}^{M-1}\frac{f_i v_i^2+f_{i+1}v_{i+1}^2}{2}\,h_{i+1}$$
$$=\sum_{i=1}^{M-1}\frac{f_i v_i^2}{2}\,h_{i+1}+\sum_{i=2}^{M}\frac{f_i v_i^2}{2}\,h_i=\sum_{i=2}^{M-1}\frac{f_i v_i^2}{2}\,h_i\,,$$

since it is assumed that $f_{M+1}=0$ and that $v_1=0$. Accordingly, the first point does not enter into the difference equation. Let us compute the change in particle number over a time step with the aid of difference equation (3.4) by summing both its parts with an appropriate weight:

$$\Delta n=\sum_{i=2}^{M-1}h_i v_i^2\left(f_i^k-f_i^{k-1}\right)=\tau\left[\frac{J_{M+1/2}^k}{v_{M+1/2}}-\frac{J_{3/2}^k}{v_{3/2}}\right].$$

Assume that $J_{M+1/2}=0$, since $f_M=0$ at the tail, and formally set $J_{3/2}=0$ (we will learn below about its implications), then $\Delta n=0$. The change in energy is given by

$$\Delta E=\sum_{i=2}^{M-1}h_i v_i^4\left(f_i^k-f_i^{k-1}\right)$$
$$=\tau\left[\frac{v_{M+1}^2}{v_{M+1/2}}\,J_{M+1/2}-\frac{v_2^2}{v_{3/2}}\,J_{3/2}-2\sum_{i=2}^{M-1}h_{i+1}J_{i+1/2}\right].$$

If we take into account that the particle number is conserved, and that the relationship

$$\sum_{i=1}^{M-1}h_{i+1}J_{i+1/2}=0$$

is valid, then $\Delta E\approx 0$. Difference equation (3.4) is written out at point $i=2$ in the following way:

$$\frac{f_i^k-f_i^{k-1}}{\tau}=\frac{1}{v_i^2 h_{i+1/2}}\,\frac{J_{i+1/2}^k}{v_{i+1/2}}\,,\quad i=2\,. \tag{3.4a}$$

We need to know the boundary condition for the distribution function at the point $i=1$, and we derive it from the condition $J_{3/2}=0$.

For a numerical solution, the finite-difference scheme is rearranged into a system of nonlinear difference equations solved at each time step and, accordingly, at each iteration by the sweep method.

Let us rewrite the scheme in a form convenient for numerical computations. To do so, the following notation is introduced:

$$\Sigma_{i+1}=\sum_{m=1}^{M-1}h_{m+1}Q_{i+1/2,m+1/2}(v_m f_m+v_{m+1}f_{m+1})\,,$$

$$\Theta_{i+1}=\sum_{m=1}^{M-1}Q_{i+1/2,m+1/2}(f_{m+1}-f_m)\,,$$

$$A_i=\frac{1}{v_{i-1/2}\,h_i}\,(\Sigma_i-v_i h_i\Theta_i)\,,\quad B_i=\frac{1}{v_{i-1/2}h_i}\,(\Sigma_i+v_i h_i\Theta_i)\,,$$

$$\alpha_i=\frac{\tau}{v_i^2 h_i}\,A_{i+1}\,,\quad \beta_i=\frac{\tau}{v_i^2 h_i}\,(A_i+B_{i+1})\,,$$

$$\gamma_i=\frac{\tau}{v_i^2 h_i}\,B_i\,,\quad \psi_i=-f_i^{k-1}\,,\quad i=2,\ldots,M-1\,.$$

The set of difference equations is then written out as

$$\alpha_i f_{i+1}-(1+\beta_i)f_i+\gamma_i f_{i-1}=\psi_i\,,\ i=2,\ldots,M-1\,, \tag{3.5}$$

with the first difference equation involving

$$\alpha_2=\frac{\tau}{v_2^2 h_i}\,A_3\,,\quad \beta_2=\frac{\tau}{v_2^2 h_i}\,B_3\,,\quad \gamma_2=0\,.$$

From the equality $J_{3/2}=0$, it follows that the functions at the initial points are linked to each other at any moment of time by the following relationship

$$f_1=f_2\left(1-v_2^2\,\frac{N_2}{E_2}\right). \tag{3.6}$$

If the boundary condition of the second kind (equaling zero of the derivative) is approximated based on the formulation of an exact problem with the first- or second-order approximation, the conservation law is not necessarily warranted. What does the approximation imply if it is derived formally from the requirement that a difference analog of the conservation law be implemented? The boundary condition arising formally proves to be quite reasonable. Consider, for definiteness, charged particles and the kernel $Q(v,w)$ corresponding to their Coulomb interactions. Suppose the distribution function is quasi-Maxwellian: $f_i^{\mathrm{M}}=C\exp(-v_i^2/v_{\mathrm{th}}^2)$. Then, estimating expression (3.4a) and neglecting terms on the order of $O(h^3)$, we find

$$f_1^{\mathrm{M}}=f_2^{\mathrm{M}}\left(1+\frac{v_2^2}{v_{\mathrm{th}}^2}\right).$$

We only note that, initially conceived as just a formality, the requirement of full conservatism leads to a more natural approximation of exact conditions in a subsequent analysis of exact initial data. We revisit this question when constructing a scheme for the Landau–Fokker–Planck equation.

Since the difference schemes are chosen implicit, the time step τ is determined by the required solution accuracy and the distribution character. The scheme is nonmonotonic; it can be made monotonic but then we have to sacrifice the second-order spatial approximation.

Since the distribution function should be nonnegative for stability and by its physical sense, the coefficients of difference equation (3.5) should satisfy the conditions α, $\gamma>0$, $1+\beta>0$, which requires $h_i=v_i-v_{i-1}$, $h_i<E_i/n_i v_i$. The Landau–Fokker–Planck equation is a parabolic one, and as $v\to\infty$ it degenerates into an almost hyperbolic equation; therefore, to account for the exponentially decreasing functions, the step should even be reduced in order to ensure accuracy. A rough discretization step estimate based on velocity, which can be over or under for particular tasks, takes the form $h<v_{\mathrm{th}}^2/nL$.

For power-law interaction potentials $U=a/r^{\beta}$, where $1<\beta<4$, the symmetric kernel $Q(v,w)$ is represented in the form [24, 25]

$$Q(v,w)=\frac{a(v,w)(v+w)^{n_1+4}+b(v,w)|v-w|^{n_1+4}}{(n_1+2)(n_1+4)(n_1+6)}\,, \tag{3.7}$$

$$a(v,w)=(n_1+4)\,vw-(v^2+w^2)\,,$$

$$b(v,w)=(n_1+4)\,vw+(v^2+w^2)\,,\quad n_1=\frac{\beta-4}{\beta}\,.$$

The negative values of n_1 correspond to soft potentials ($1 \leqslant \beta \leqslant 4$). For charged particles, one has $\beta = 1$ ($n_1 = -3$).

To illustrate the performance of the difference scheme, the initial distribution is chosen as a δ-function which is approximated in the following manner:

$$f(v_i, 0) = \begin{cases} \dfrac{2}{v_{i+1} - v_{i-1}}, & v_i = 1, \\ 0, & v_i \neq 1. \end{cases}$$

Such an approximation models the difference delta function; relatedly, both the number density and energy of particles become equal to unity. We limit ourselves to only presenting results of simulation for this type of initial distribution.

A relaxation of initial distribution to the equilibrium state belongs to classical problems of plasma physics and is among the test problems for any model of collisional plasma.

Moving along, we note that the particle number density is preserved with a machine accuracy (random error), while the energy depends on the accuracy of δ iterations because of the nonlinearity of the equation. For $\delta = 10^{-3}$, the relative error makes $\Delta\varepsilon = 10^{-2}\%$, and for $\delta = 10^{-7}$, it is $\Delta\varepsilon = 10^{-5}\%$, i.e., the energy error does not exceed 10^{-7}. Such a level of accuracy is needed, for example, in exploring asymptotic problems.

Finite initial conditions are considered at $t = 0$, with the initial function $f_0(v) = f(v, 0)$ being confined to the thermal range $v \approx v_{\text{th}}$.

At long times, when the relaxation in the thermal domain is completed, the equation can be considered as a linear one in the hot domain for $v \gg v_{\text{th}}$:

$$\frac{\partial f}{\partial t} = \frac{n}{8} \frac{1}{v^2} \frac{\partial}{\partial v} \left[v^3 \sigma(v) \left(\frac{T}{m} \frac{\partial f}{\partial v} + vf \right) \right].$$

Here, we took into account that in the hot domain the kernel $Q(v, w) \to \pi w^3 v^4 \sigma(v)/6$ as $v \to \infty$, and used the scattering cross section $\sigma(u, \mu) = g_\beta(\mu)\, u^{-4/\beta}$ [22–25] for the power-law interaction potential. Substituting the expression for $Q(v, w)$ into Eqn (3.3), for $v \gg v_{\text{th}}$ we arrive at the final form of the last equation:

$$\frac{\partial f}{\partial t} = \frac{n g_\beta}{8} \frac{1}{v^2} \frac{\partial}{\partial v} \left[v^{3-4/\beta} \left(\frac{T}{m} \frac{\partial f}{\partial v} + vf \right) \right], \tag{3.8}$$

where the following notation was introduced:

$$g_\beta = 2\pi \int_{-1}^{1} \mathrm{d}\mu\, g_\beta(\mu)(1 - \mu^2). \tag{3.9}$$

For example, formula (3.9) for the Coulomb potential ($\beta = 1$) gives $g_1 = 32\pi e^4 L/m$. In this case, Eqn (3.8) reduces to the well-known linear Landau–Fokker–Planck equation for plasmas.

Further, let us consider equation (3.8) for arbitrary potentials $U = \alpha/r^\beta$, $1 \leqslant \beta < 4$. The finite-difference scheme has already been presented above. For the chosen variables, the conservation laws for the particle number density and energy look like

$$n = \int_0^\infty v^2\, \mathrm{d}v f(v, t) = 1, \quad E = \int_0^\infty v^4\, \mathrm{d}v f(v, t), \quad t \geqslant 0. \tag{3.10}$$

The thermal velocity $v_{\text{th}} = 1$, and the equilibrium solution is written down as

$$f_{\text{M}}(v) = \frac{4}{\pi^{1/2}} \left(\frac{3}{2} \right)^{3/2} \exp\left(-\frac{3}{2} v^2 \right).$$

At the initial moment of time, the function is the delta function $f(v, 0) = \delta(v - 1)/v^2$ confined in the thermal domain. When choosing the boundary L for the velocity interval, hot particles are estimated from the Maxwell distribution, which yield $L \approx (7-8)\, v_{\text{th}}$. The difference scheme expressed by formula (3.5) is used. The initial function is approximated as mentioned above. For this approximation, the number of particles equals one, and the kinetic energy $v_i^2 = 1$.

We present below the results of modeling. The function smears over the thermal domain ($0 < v < 2$) rather rapidly and then becomes monotonic, attaining its maximum at zero at a certain moment t_0 which corresponds to the so-called collisional time. This characteristic time t_0 is only weakly dependent on the exponent β in the expression for the particle interaction potential $U = \alpha/r^\beta$. In this domain, the distribution functions for different exponents stay rather close to each other during the entire relaxation process for various potentials. The distinction is more prominent in the hotter domain with $v > 2$ and at distribution tails. To make the presentation of results more explicit, the function normalized on the Maxwell distribution, $g(v, t) = f(v, t)/f_{\text{M}}(v)$, is introduced. Figures 1–3 plot the graphs of function $f(v, t)$ in the velocity interval $2 < v/v_{\text{th}} < 5$ for different time moments and values of the parameter β. All curves demonstrate the wave character of propagation of $g(v, t)$ toward the domain of high velocities. For the Coulomb interaction ($\beta = 1$, $n_1 = -3$, $U = \alpha/r$), the function $g(v, t)$ is shown in Fig. 1. The solution has the character of a wave propagating with a stable (stiff) front. For the particle interaction potentials with $1 < \beta < 2$, the tail relaxation proceeds more slowly than the relaxation of the distribution core. Beginning with $2 < \beta < 3$, the tail evolution gradually loses the wave character. Figure 2 demonstrates that the wave front slowly rises with time ($\beta = 2$, $n_1 = -1$, $U = \alpha/r^2$). For stiff potentials ($\beta > 4$), the characteristic relaxation times for the distribution core and

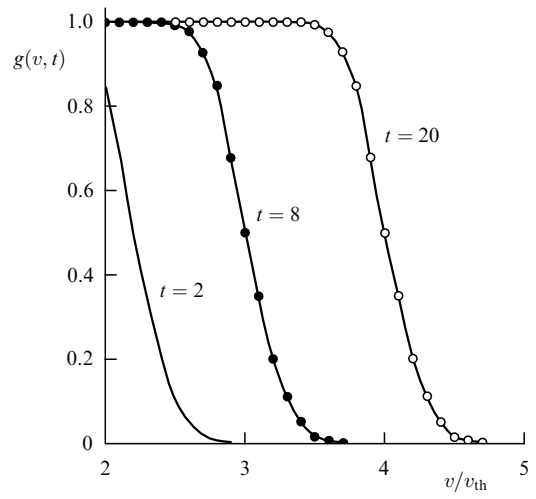

Figure 1. Plots of the distribution function normalized to the Maxwell distribution, $g(v, t) = f(v, t)/f_{\text{M}}(v)$, for velocities in the range $2 < v/v_{\text{th}} < 5$ for several moments of time t (in arbitrary units). The time is normalized on the time of electron–electron collisions (3.11). Plots correspond to the case of Coulomb interactions: $n_1 = -3$, $\beta = 1$, $U = \alpha/r$.

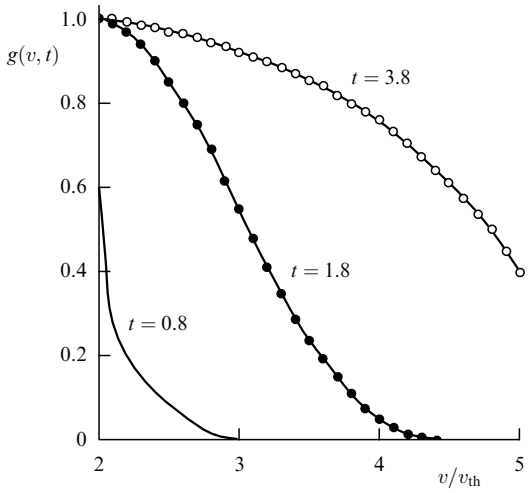

Figure 2. Plots of the distribution function normalized to the Maxwell distribution, $g(v,t) = f(v,t)/f_{\rm M}(v)$, for velocities in the range $2 < v/v_{\rm th} < 5$ for several moments of time t (in arbitrary units). The time is normalized on the time of electron–electron collisions (3.11). Plots correspond to the case of dipole interactions: $n_1 = -1$, $\beta = 2$, $U = \alpha/r^2$.

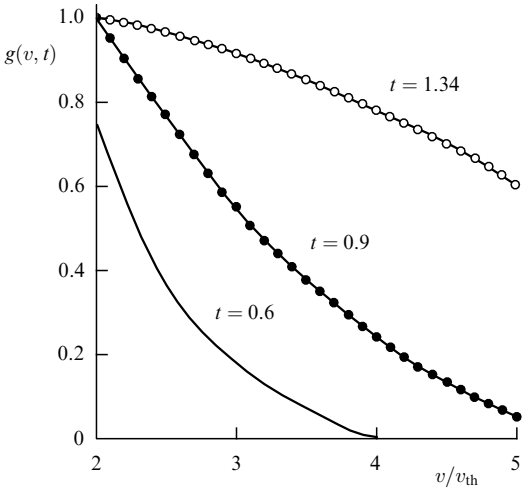

Figure 3. Plots of the distribution function normalized to the Maxwell distribution, $g(v,t) = f(v,t)/f_{\rm M}(v)$, for velocities in the range $2 < v/v_{\rm th} < 5$ for several moments of time t (in arbitrary units). The time is normalized on the time of electron–electron collisions (3.11). Plots correspond to the case of interactions of Maxwell molecules: $n_1 = 0$, $\beta = 4$, $U = \alpha/r^4$.

tail are practically indistinguishable (times of 1–2). As a consequence, the velocities of propagation and smearing are hardly distinguishable (Fig. 3), and the relaxation in thermal and hotter domains occurs simultaneously.

As can be concluded, the front width $\Delta_{\rm f}(t)$ is essentially dependent on the power-law exponent β in the interaction potential. Indeed, $\Delta_{\rm f}(t)$ takes a constant value for $1 < \beta < 2$, i.e., the propagation of $g(v,t)$ in this case has the character of a wave with a stable profile, which does not smear with time for $t > 0$. This fact was discovered numerically at $\beta = 1$ in Refs [22–25], and the respective analytical solution was developed. Beginning from the exponent $\beta = 2$, the front starts to slightly smear out, following a weak logarithmic dependence on time: $\Delta_{\rm f}(t) \propto \sqrt{\ln t}$. The solution should preserve its wave character. The propagation speed $v_{\rm f}(t)$ of a front is higher than the rate of its smearing.

To facilitate the analysis, equation (3.8) is recast in a convenient form by introducing dimensionless variables for the velocity, time, and distribution function:

$$x = \left[\frac{v}{v_{\rm th}}\right]^{(4+\beta)/2\beta} X^{(4+\beta)/2\beta}, \quad \tau = t\,\frac{\rho g_\beta}{8}\,\frac{4-\beta}{\beta}\left[\frac{X}{v_{\rm th}}\right]^{(4-\beta)/2\beta}, \tag{3.11}$$

$$f(v,t) = f_{\rm M}(v)\,u(x,\tau)\,,$$

where $X = 2\beta(4-\beta)/(4+\beta)^2$, and $f_{\rm M}(v)$ is the Maxwell distribution function. Substituting representation (3.11) into Eqn (3.8), we obtain the equation for the distribution function $u(x,\tau)$ in dimensionless variables:

$$\frac{\partial u}{\partial \tau} + \frac{x^{1-p}}{p}\,\frac{\partial u}{\partial x} = \frac{1}{2}\,\frac{\partial^2 u}{\partial x^2}\,, \quad p = 2\,\frac{4-\beta}{4+\beta}\,. \tag{3.12}$$

The type of the last equation gives an idea about the wave character of its solution. Indeed, it is worth mentioning that we are interested in the hot domain $x \gg 1$ and the times at which $u(x,\tau) \approx 1$ and slow establishment of the equilibrium solution $u_{\rm M}(x) = 1$ occurs at tails, while $u(x,\tau) \to 0$ as $x \to \infty$. The condition $x \gg 1$ will be taken into account with the aid of new variables $\tilde{x} = x/x_0$ and $\tilde{\tau} = \tau/x_0^p$, where $x_0 \gg 1$ is some characteristic scale. In this case, equation (3.12) acquires a small parameter $x_0^{p-2} \ll 1$ of the higher derivative. Hence, it follows that the Landau equation changes its type in $x \to \infty$ tails and becomes a transport operator. Taking this into account, we introduce a formal parameter ε of the second derivative. We obtain, as a result, that

$$\frac{\partial u}{\partial \tau} + \frac{x^{1-p}}{p}\,\frac{\partial u}{\partial x} = \frac{\varepsilon}{2}\,\frac{\partial^2 u}{\partial x^2}\,. \tag{3.13}$$

At $\varepsilon \approx 0$, the last equation reduces to a first-order equation, and the equilibrium solution $u_{\rm M}(x)$ is simply carried along its characteristics. The typical solution of equation (3.13) has the form of a step function:

$$u(x,\tau) \approx \theta(\tau^{1/p} - x)\,, \quad p = 2\,\frac{4-\beta}{4+\beta}\,. \tag{3.14}$$

Approximate solution (3.14) properly reflects the asymptotic law followed by the wave front, $x_{\rm f}(\tau) \propto \tau^{1/p}$, but does not describe the front structure. In order to analyze it, equation (3.13) is transformed with due regard for the information on the wave front behavior obtained earlier. Introducing new variables

$$z = \frac{x - \tau^{1/p}}{\sqrt{\varepsilon}}\,, \quad u(x,\tau) = \phi(z,\tau)\,,$$

we rewrite equation (3.13) for the new function $\phi(z,\tau)$ as

$$\frac{\partial \phi}{\partial \tau} = \frac{1}{2}\left\{\frac{\partial^2 \phi}{\partial z^2} - \frac{2}{p}\,\frac{\tau^{1/p} - 1}{\sqrt{\varepsilon}}\left[\left(1 + \sqrt{\varepsilon}\,\frac{z}{\tau^{1/p}}\right)^{1-p} - 1\right]\frac{\partial \phi}{\partial z}\right\}. \tag{3.15}$$

Suppose ε is small but retain z finite. In this conditional limit, formula (3.15) reduces to

$$\frac{\partial \phi}{\partial \tau} = \frac{1}{2}\left(\frac{\partial^2 \phi}{\partial z^2} - \gamma\,\frac{z}{\tau}\,\frac{\partial \phi}{\partial z}\right), \quad \gamma = 2\,\frac{1-p}{p}\,. \tag{3.16}$$

The boundary conditions for the function $\phi(z,\tau)$ are as follows: $\phi \to 1$ when $z \to -\infty$ (behind the front), and $\phi \to 0$ when $z \to 0$ (ahead the front). The function $\phi(z,\tau)$ is constructed as a solution to the initial value problem for time $\tau > 1$ with the respective initial condition $\phi(z,1) = \theta(-z)$ [cf. function (3.14)]. By an appropriate variable change, equation (3.16) reduces to the heat conduction equation [24, 25]. As a result, a self-similar solution to equation (3.16) is obtained:

$$\phi(z,\tau) = \Phi\left[z\sqrt{\frac{1-\gamma}{2(\tau-\tau^{\gamma})}}\right], \quad \tau > 1,$$
$$\Phi(z) = \frac{1}{\sqrt{\pi}}\int_z^{\infty} \mathrm{d}y\, \exp(-y^2). \tag{3.17}$$

Returning to the variable x and recalling that $\varepsilon = 1$, we find the quasistationary solution to equation (3.17):

$$u(x,\tau) \approx \Phi\left[\frac{x-\tau^{1/p}}{\sqrt{2}}\sqrt{\frac{1-\gamma}{\tau-\tau^{\gamma}}}\right], \quad \tau > 1, \quad \gamma = 2\,\frac{1-p}{p}. \tag{3.18}$$

In order to learn where solution (3.18) is valid, let us formulate all the assumptions made en route. The kinetic equation is considered for $x \gg 1$ and a large time (larger than the Coulomb collision time) $\tau \gg 1$ close to the wave front $x_{\mathrm{f}}(\tau) \propto \tau^{1/p}$, $x - \tau^{1/p} \ll \tau^{1/p}$. The last inequality justifies the passage from Eqn (3.15) to Eqn (3.16), subject to the condition $\varepsilon = 1$, and leads to the following constrains. The derived solution (3.18) is inapplicable, first, in the interval $0 < x \ll x_{\mathrm{f}}$, and, second, for particles outside the region $x > 2x_{\mathrm{f}}$. Neither case is interesting from a practical viewpoint because, with a good accuracy, it can be assumed that $u(x,\tau) \approx 1$ in the first region $x \ll x_{\mathrm{f}}(t)$, and $u(x,\tau) \approx 0$ in the second region $x \geqslant 2x_{\mathrm{f}}$. Formula (3.18) can be simplified with account for the condition $\tau \gg 1$. Since the final result depends on γ, three cases may be considered for the expression under the radical sign in formula (3.18). The expression $(1-\gamma)(\tau-\tau^{\gamma})^{-1}$ for $\gamma < 1$ tends to $(1-\gamma)\,\tau^{-1}$, and for $\gamma > 1$ it tends to $(\gamma-1)\,\tau^{-\gamma}$. The case of $\gamma = 1$ is a boundary one and is different from the other cases. Notice that $\gamma = 1$ corresponds to $\beta = 2$, i.e., the dipole interaction between particles. In this limiting case, the expression is rewritten as

$$(1-\gamma)(\tau-\tau^{\gamma})^{-1} = (1-\gamma)\left(\tau^{\gamma}\sum_{i=1}^{\infty}\frac{\left[(1-\gamma)\,\ln\tau\right]^i}{i!}\right)^{-1}.$$

The last expression contains only the first term at $\gamma = 1$, because the coefficients of the sum disappear for all $i > 2$.

Thus, simplified expressions for the asymptotic solution $u(x,\tau)$, which is a function of the exponent γ, are arrived at under the condition $\tau \gg 1$:

$$u(x,\tau) = \Phi\left\{\frac{x-\tau^{1/p}}{\sqrt{2}}\sqrt{\frac{1-\gamma}{\tau}}\right\}, \quad \gamma < 1;$$
$$u(x,\tau) = \Phi\left\{\frac{x-\tau^{1/p}}{\sqrt{2}}\sqrt{\frac{1}{\tau\ln\tau}}\right\}, \quad \gamma = 1; \tag{3.19}$$
$$u(x,\tau) = \Phi\left\{\frac{x-\tau^{1/p}}{\sqrt{2}}\sqrt{\frac{\gamma-1}{\tau}}\right\}, \quad \gamma > 1.$$

Finally, we reformulate the results obtained above in terms of original variables v, t, and for the distribution function $f_\beta(v,t)$:

$$f_\beta(v,t) \approx n\left(\frac{m}{2\pi T}\right)^{3/2}\exp\left(-\frac{mv^2}{2T}\right) \times u\left(v\sqrt{\frac{m}{T}},\ t\,\frac{\rho g_\beta}{8}\left(\frac{m}{T}\right)^{(4-\beta)/2\beta}\right). \tag{3.20}$$

The constant factor g_β is defined by formula (3.9). The function $u(v,t)$ has the form of a propagating wave, the front of which travels according to the law

$$v_{\mathrm{f}}(t) = \left(\frac{4-\beta}{\beta}\right)^{\beta/(4-\beta)}.$$

The function $u(v,t)$ is described by three expressions depending on the value of the exponent β:

$$u(v,t) = \Phi\left\{2\,\frac{\sqrt{\beta(2-\beta)}}{4+\beta}\,v_{\mathrm{f}}V^{(4+\beta)/2\beta}\right\}, \quad 1 \leqslant \beta < 2;$$
$$u(v,t) = \Phi\left\{\frac{1}{3}\,(\ln v_{\mathrm{f}})^{-1/2}v_{\mathrm{f}}V^{3/2}\right\}, \quad \beta = 2; \tag{3.21}$$
$$u(v,t) = \Phi\left\{\sqrt{\frac{2(\beta-2)}{4-\beta}}\left[\frac{2\beta(4-\beta)}{4+\beta}\right]^{(4-\beta)/2\beta} \times v_{\mathrm{f}}^{(4+\beta)/\beta}V^{(4+\beta)/2\beta}\right\}, \quad 2 < \beta < 4,$$

where $V = (v - v_{\mathrm{f}}(t))/v_{\mathrm{f}}(t)$.

The usability conditions for solution (3.21) have the form of strong inequalities:

$$v \gg 1, \quad v_{\mathrm{f}}(t) \gg 1, \quad \left|v - v_{\mathrm{f}}(t)\right| \ll v_{\mathrm{f}}(t).$$

Notice that $u\bigl(v_{\mathrm{f}}(t),t\bigr) = 1/2$. As usual, we define the front width in the following form

$$\Delta_{\mathrm{f}}(t) = 2\left|\frac{u(v,t)}{\partial u(v,t)/\partial v}\right|_{v=v_{\mathrm{f}}} = \left|\frac{\partial u(v,t)}{\partial v}\right|^{-1}_{v=v_{\mathrm{f}}}.$$

Consequently, for the cases considered above we obtain

$$\Delta_{\mathrm{f}}(t) = \sqrt{\frac{\pi\beta}{2-\beta}}, \quad 1 \leqslant \beta < 2;$$
$$\Delta_{\mathrm{f}}(t) = \sqrt{\pi\ln v_{\mathrm{f}}(t)}, \quad \beta = 2; \tag{3.22}$$
$$\Delta_{\mathrm{f}}(t) = \sqrt{\frac{\pi\beta}{2-\beta}\,\frac{2\beta(4-\beta)}{(4+\beta)^2}}\left[v_{\mathrm{f}}(t)\right]^{2(\beta-2)/\beta}, \quad 2 < \beta < 4.$$

It can be seen that the front width $\Delta_{\mathrm{f}}(t)$ essentially depends on the exponent β in the interaction potential. Thus, $\Delta_{\mathrm{f}}(t)$ takes a constant value for $1 < \beta < 2$. The propagation of $u(v,t)$, in this case, has the character of a wave with a stable profile which is left unsmeared with time for $t > 0$. For $\beta \geqslant 2$, the front gradually smears out, showing a weak logarithmic dependence $\Delta_{\mathrm{f}} \propto \sqrt{\ln t}$. The solution behavior should still preserve its wave character. The front propagation speed exceeds the rate at which it is smeared out:

$$\frac{\partial\Delta_{\mathrm{f}}/\partial t}{\partial v_{\mathrm{f}}/\partial t} = \frac{\mathrm{d}\Delta_{\mathrm{f}}}{\mathrm{d}v_{\mathrm{f}}}.$$

3.2 Numerical modeling of the formation of nonequilibrium particle distribution functions for stationary self-consistent sources and sinks

In this section, we analyze the formation of nonequilibrium quasistationary distribution functions in a spatially homogeneous isotropic plasma composed of one kind of particles, in the presence of localized sources (sinks) of particles (energy) in velocity space. The existence of nonequilibrium distribution functions assumes the presence of sources and sinks in momentum space. An energy (particle) source and sink can be maintained by ion beams, powerful laser radiation, emission current, beams of charged particles emitted in fusion or fission reactions, etc. The analysis is based on the Landau–Fokker–Planck equation, which is a model of the Boltzmann equation for arbitrary interaction potentials of particles [21–26].

We concentrate now on a numerical study of the evolution of nonequilibrium distribution functions and their dependence on various input parameters — the intensity of sources, the degree of their localization in velocity space, and so forth. Section 4 compares results simulated numerically with those obtained in a particular experiment dealing with the irradiation of a semiconductor by fast ions [29–32]. Fully conservative difference schemes [22–28] are applied for numerical modeling.

Numerical implementation of the problem solved here faces a fundamental difficulty rooted in the nonlinearity of the collision integral. As has already been mentioned, two conservation laws should be obeyed in the absence of external sources; otherwise, the dissipative properties of the difference scheme may distort the result through the influence of implicit sinks or sources. For this reason, numerical schemes capable of appropriately handling the nonlinearity of the modelled equation are employed [26].

Nonlinear operator (3.3) with the symmetric kernel $Q(v, w)$ for power-law interaction potentials (3.7) is utilized in numerical modeling. For charged particles $\beta = 1$ ($n_1 = -3$), so then $Q(v, w) = (2/3)\, w^3$ for $w < v$, and $Q(v, w) = (2/3)\, v^3$ for $w > v$.

Following a common procedure of making equations dimensionless, we change to the variables

$$v' = \frac{v}{v_{\rm th}}\,; \quad t' = \frac{\tilde{t}}{t_\beta}\,, \quad t_\beta = \frac{32\pi v_{\rm th}^3}{n g_\beta}\, v_{\rm th}^{4(\beta-1)/\beta};$$
$$f' = \frac{4\pi v_{\rm th}^3}{n} f; \quad S' = \frac{4\pi v_{\rm th}^3 t_S S}{n_S}\,. \tag{3.23}$$

To implement the difference scheme, the infinite interval in velocity space is replaced by a finite interval $[0, v_{\max}]$ selected so as to account for high-energy particles, and the boundary condition for the distribution function is taken as $f(v_{\max}, t) = 0$. The sources S_+ and sinks S_- in most cases are chosen as δ-functions:

$$S_\pm = \frac{I_\pm\, \delta(v - v_\pm)}{v^2}\,. \tag{3.24}$$

If the intensities of a source and sink satisfy the relationship $I_+ = I_- v_-^2 / v_+^2$, the energy acquired by the system from outside equals zero, but the particle density in the system decreases (if the source is associated with larger velocities than the sink), i.e., in this situation an analog of constant energy flux in momentum space is realized with nonconservation of particle density in the system. Since we are dealing with charged particles, as the electron density drops in a certain region, thermal electrons from its surroundings tend to replenish it, driven by the arising electric field. In the framework of the spatially homogeneous model considered here, this can be taken into account by introducing yet another source with an intensity $I_{\rm th}$ so as to compensate for the decrease in particle number and, respectively, the generation of the electric field. In this manner, we can formulate a consistent model with two sources of intensities I_+ and $I_{\rm th}$ and one sink of intensity I_-, in the framework of which neither the energy nor the particle density will change. This will be achieved if the intensities of sources and sinks satisfy the two relationships

$$I_{\rm th} - I_- + I_+ = 0\,, \quad I_{\rm th} v_{\rm th}^2 - I_- v_-^2 + I_+ v_+^2 = 0\,. \tag{3.25}$$

They can be rewritten as the expressions for the intensities of sources in terms of the sink intensity I_-:

$$I_+ = I_- \frac{v_-^2 - v_{\rm th}^2}{v_+^2 - v_{\rm th}^2}\,, \quad I_{\rm th} = I_- \frac{v_+^2 - v_-^2}{v_+^2 - v_{\rm th}^2}\,. \tag{3.26}$$

Additionally, in numerical computations we will sometimes consider sources (sinks) which are distributed exponentially over velocities:

$$S_\pm \propto I_\pm \exp\left[-b(v - v_\pm)^2\right]. \tag{3.27}$$

Such an expression for the source or sink proves to be convenient for exploring the dependence of nonequilibrium distribution functions on the source shape. We remark that, strictly speaking, the introduction of sinks which are independent of the distribution function may face severe problems. In this arrangement, one may specify such initial conditions that solutions will become negative in the vicinity of the sink as time progresses. For this reason, the sources (sinks) are frequently modelled by terms that are proportional to the distribution function sought after, namely

$$S_\pm = I_\pm \frac{\delta(v - v_\pm)}{v^2}\, f(v, t)\,. \tag{3.28}$$

It will be recalled that in the discrete case the function $\delta(v - v_1)$ differs from zero only at $v = v_1$. The initial distribution is chosen as Maxwellian or δ-functional. It should be noted that results are practically insensitive to the shape of the initial distribution function, except for the very initial stage. Iterations are carried out on each time step, the particle number is preserved up to the machine precision, and the energy is conserved up to 7–8 significant figures.

Later, we discuss the main results of numerical simulations in the presence of particle or energy fluxes in momentum space [29–31]. There are the source S_+ and sink S_- on the right-hand side of kinetic equations (3.3) to maintain the flux in momentum space. We begin with the case when the source and sink conform in momentum space with the direction of flux transferred as a result of collisions. Notice that analytical consideration of equations for a localized source and sink gives the correct flux direction — from high to low velocities. It can be seen from Fig. 4 that, as time progresses, a nonequilibrium stationary (Kolmogorov type) particle distribution is established in the interval between the source and sink, in agreement with the presence of energy flux in momentum space, while outside this interval the distribution function remains a thermodynamically equilibrium one. To convince ourselves once again that the location of source and

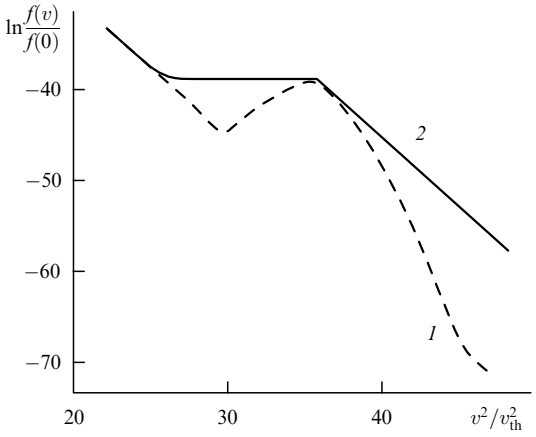

Figure 4. Dependence of the logarithm of the nonequilibrium stationary distribution function normalized to its value at $v = 0$ on the dimensionless velocity squared. The computations use the initial Maxwell distribution function and the source function with $I = 10^{-16}$, $v_- = 5$, $v_+ = 6$, and are carried out for the Landau–Fokker–Planck equation at the instants of time $t_2 = 100$ (solid line) and $t_1 = 25$ (dashed line).

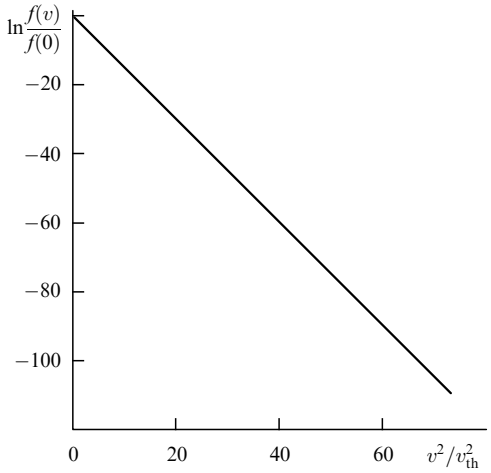

Figure 5. Dependence of stationary (equilibrium) distribution function for nonconforming location of the source and sink, $v_+ = 5$, $v_- = 7$, obtained from computations based on the Fokker–Planck and also the Landau equations for $\beta = 1, 2, 3$.

sink need to conform with the flux direction in momentum space, we carried out computations with opposite locations of the source and sink in energy space. Figure 5 displays the logarithm of distribution function versus (dimensionless) velocity squared for the incorrect arrangement of the source and sink. Apparently, the particle distribution function stays in thermodynamic equilibrium as the flux intensity is varied over several orders of magnitude — this reinforces the importance of conforming the placement of a source and sink.

For the variant presented in Fig. 6, the functional dependence of the source and sink on velocity is exponential. The source S_+ occupies a 'narrow' domain in the vicinity of energies that corresponds to seven thermal velocities, while the sink S_- is also sufficiently local in the region of four thermal velocities. The localization regions of the source and sink are controlled by the value of coefficient α_1 in the exponential function. In the case considered, the coefficient α_1 is fairly large (it equals 100), which ensures their strong localization. We explore the dependence of the electron distribution function on the degree of source and sink localization in energy space. With this aim, the magnitude of coefficient α_1 was reduced in the next simulations by one order to $\alpha_1 = 10$. From the comparison of results presented in Figs 6 and 7, it can be concluded that the character of the nonequilibrium stationary distribution in the main domain between the source and sink does not depend on the degree of source (sink) localization, which witnesses in favor of the locality of the distribution function.

Figure 8 plots the dependence of distribution functions on the square of the dimensionless velocity for various flux intensities. It is found that for small intensities of source I_+ (sink I_-), the universal nonequilibrium distribution is formed in the vicinity of velocities $v \leqslant v_+$, which is caused, first, by a reduction in the Coulomb scattering cross section as velocity is increased ($\sim v^{-3}$) and, second, by the always existing flux of energy and particles (because of the Coulomb diffusion) into the region of the basic, 'background' equilibrium distribution function. For this reason, as the intensity is increased, the universal nonequilibrium particle distribution forms, tending to occupy an ever larger region between the source and sink, which is related to the reduction in the relative role of the flux

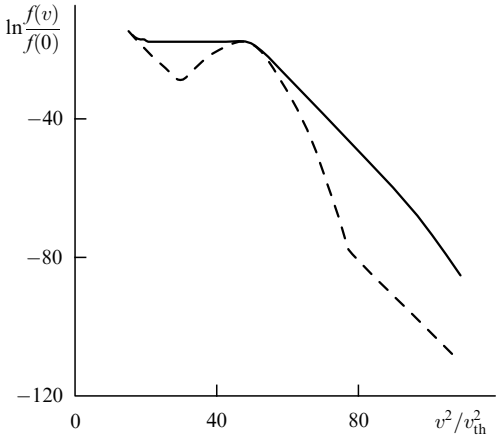

Figure 6. Distribution function computed from the Fokker–Planck equation for the source (sink) $S_\pm \sim I_\pm \exp\{-\alpha_1 (v - v_\pm)^2\}$, $\alpha_1 = 100$, $v_- = 4$, and $v_+ = 7$. The dashed and solid lines correspond to time moments $t = 25$ and $t = 100$, respectively.

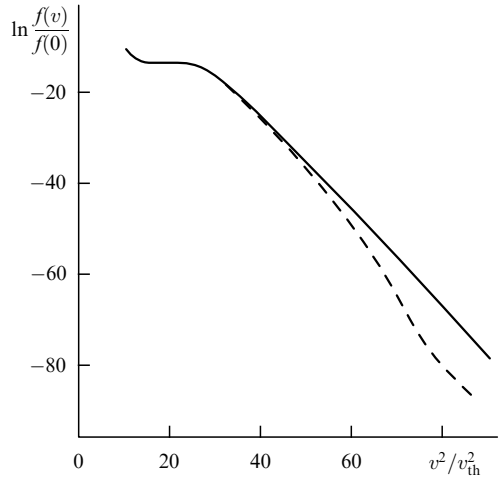

Figure 7. Distribution function computed from the Fokker–Planck equation for the source (sink) $S_\pm \sim I_\pm \exp\{-\alpha_1 (v - v_\pm)^2\}$, $\alpha_1 = 10$, $v_- = 3$, and $v_+ = 5$. The dashed and solid lines correspond to time moments $t = 25$ and $t = 100$, respectively.

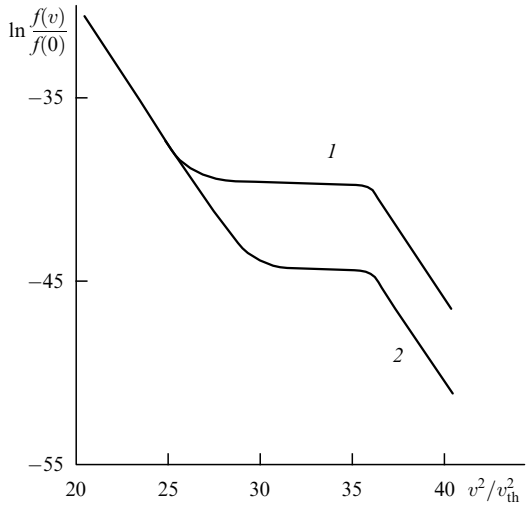

Figure 8. Stationary distribution function obtained from the Landau equation at $\beta = 2$ for a source (sink) in the form of δ-function (3.24) for various flux intensities $I = 0.01$ (*1*), 0.001 (*2*) and $v_- = 4$, $v_+ = 6$.

leaving for (transferred to) the 'background' plasma. It is worth noting that the magnitude of the nonequilibrium distribution function grows together with the intensity, since it is proportional to the magnitude of flux (2.6). Some numerical values of the nonequilibrium stationary distribution function obtained by solving the Landau equation are listed in Tables 1 and 2. The results present a detailed study of the dependence of the solution on the flux intensity, which varies in wide limits in momentum space. Function (3.24) was chosen to describe the source (sink) of particles: the sink was located at the point $v_- = 4$, and the source at $v_+ = 8$, and $\Delta E = 0$. The last equality implies that the energy flux remained constant in momentum space; however, since additional sources in the thermal domain were not involved, the particle density did not stay constant.

From Table 1 it can be seen that the amplitude of the distribution function increases with the intensity I of the flux produced by the source and sink. At low intensities (up to 0.1), the values of the distribution function grow proportionally to I, because a large contribution comes from the interaction of nonequilibrium particles (i.e., particles from the interval between the source and sink) with 'background' particles which are described by the thermodynamically equilibrium distribution function. For intermediate intensities (from 0.1 to 20), the distribution function is the universal one throughout the interval between the source and sink and is proportional to the square root of flux intensity, in agreement with expression (2.6). At large intensities, the distribution function ceases to exhibit this proportionality, because the sink intensity itself depends on the distribution function, in agreement with the chosen model of sink (3.28).

Consider the formation of the nonequilibrium particle distribution function, which corresponds to a constant energy ($\Delta E = 0$, $I_+ = I_- v_-^2/v_+^2$) or particle ($\Delta N = 0$, $I_+ = I_-$) flux. To facilitate the comparison of results, it is convenient to plot the distribution function normalized on its value at zero (Fig. 9). It can be seen that for fluxes of both particles and energy, gradually decaying distributions are formed, characterized by close exponents s.

It is interesting to learn about the form of the distribution function for various laws of interaction between particles.

Table 1.

I	$f(3.95)$	$f(7.95)$	$f(8)$
10	0.393×10^{-9}	0.417×10^{-10}	0.417×10^{-10}
1	0.475×10^{-9}	0.144×10^{-10}	0.144×10^{-10}
0.1	0.508×10^{-9}	0.189×10^{-11}	0.189×10^{-11}
0.01	0.517×10^{-9}	0.197×10^{-12}	0.197×10^{-12}
0.001	0.518×10^{-9}	0.198×10^{-13}	0.198×10^{-13}
0.0001	0.519×10^{-9}	0.196×10^{-14}	0.196×10^{-14}

Table 2.

β	1	1.5	2	3	4
$f(8)$	0.197×10^{-12}	0.123×10^{-13}	0.266×10^{-14}	0.771×10^{-15}	0.384×10^{-15}

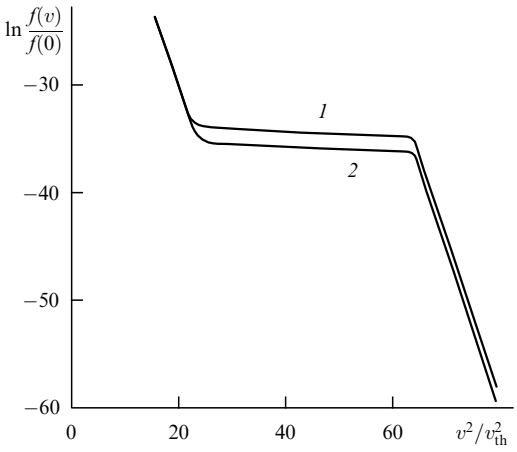

Figure 9. Stationary distribution function derived from the Landau equation at $\beta = 1$ for the source (sink) in the form of the δ-function (3.24); $|I_\mp| = 0.01$, $v_- = 4$, and $v_+ = 8$. Curves *1* and *2* correspond to constant energy ($\Delta E = 0$) and particle ($\Delta N = 0$) fluxes, respectively.

The values of the power-law exponents from the interval $1 \leqslant \beta \leqslant 4$ are considered. It should be kept in mind that $\beta = 1$ corresponds to the Coulomb interaction potential, $\beta = 2$ corresponds to the dipole interaction, and $\beta = 4$ describes the interaction of the so-called Maxwell molecules.

Table 2 presents the dependence of the distribution function $f(v_+)$ on the exponent β of interparticle interaction potential for $I = 0.01$. It is evident that for equal intensities of the source and sink, the values of the distribution function at the same value of velocity decrease, as the parameter β is increased, by almost three orders of magnitude. Figure 10 displays nonequilibrium distribution functions for the constant energy flux of intensity $I = 0.001$ (the sink and source are of the form (3.28), and are located at $v_- = 4$ and $v_+ = 8$ points, respectively), and the exponents $\beta = 1$, 2, 3. It is apparent that nonequilibrium distribution functions with close values of power-law exponents s are formed for all these values of β, which agrees with the conclusions of Ref. [30]. The absolute value of the distribution function in the nonequilibrium region drops as the exponent β is increased. These results are in qualitative agreement with the analytical results presented above.

Next, consider the evolution of the distribution function in the framework of the above-described self-consistent, spatially homogeneous model with two sources of intensities I_- and $I_{\rm th}$ and one sink with intensity I_-, in which the energy

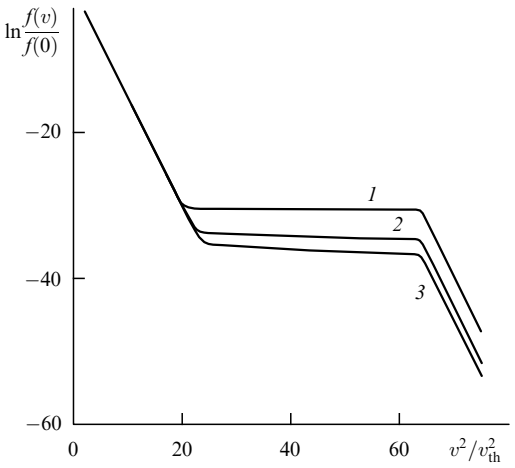

Figure 10. Dependence of nonequilibrium stationary distribution functions on velocity squared for a constant energy flux with the intensity $I = -0.01$, for the source (sink) in the form (3.28) and $v_- = 4$, $v_+ = 8$. The curves are computed from the Landau equation for the exponent $\beta = 1$ (*1*), 2 (*2*), and 4 (*3*).

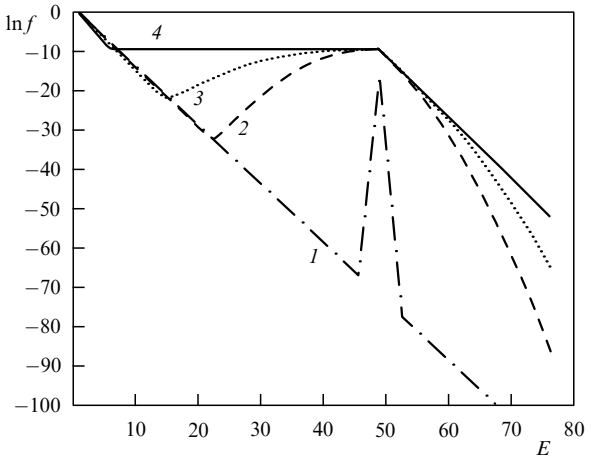

Figure 12. Energy dependence of the logarithm of the nonequilibrium distribution function obtained from the Landau equation at $\beta = 1$ for the source and sink in the form of the δ-function (3.24), $I_- = -0.002$, $v_- = 2$, $v_{1+} = 1$, $v_{2+} = 7$ at various time moments $t = 0.001$ (*1*), 10 (*2*), 20 (*3*), and 200 (*4*).

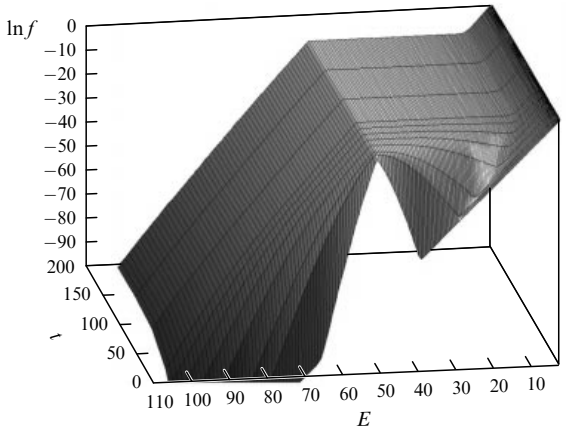

Figure 11. Time evolution of nonequilibrium distribution function computed from the Landau equation at $\beta = 1$ for the source and sink in the form of the δ-function (3.24); $I_- = -0.001$, $v_- = 2$, $v_{1+} = 1$, $v_{2+} = 7$.

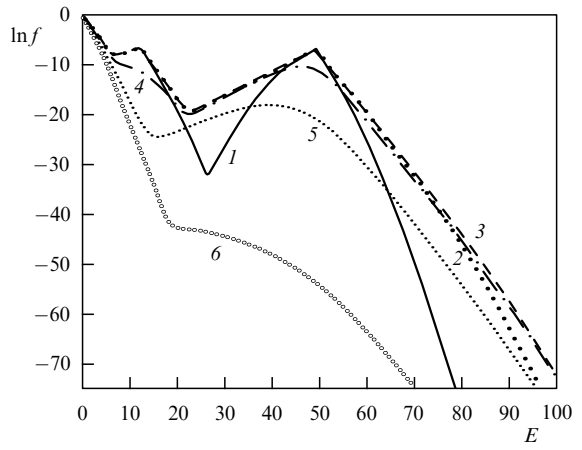

Figure 13. Evolution of the distribution function under the action of nonstationary sources and a stationary distributed sink at several time moments $t = 5$ (*1*), 20 (*2*), 30 (*3*), 35 (*4*), 50 (*5*), and 100 (*6*). Time moment $t = 30$ corresponds to switching the sources off. The sources with equal intensities $I_{1,2} = 0.01$ are localized at velocities $v_{1+} = 3.5$ and $v_{2+} = 7.0$; the sink is proportional to the distribution function and operates in the range $v_- \geqslant 2$.

and particle density do not vary with time. The intensities of sources expressed in terms of the sink intensity I_- satisfy relationships (3.26):

$$I_+ = I_- \frac{v_-^2 - v_{\rm th}^2}{v_+^2 - v_{\rm th}^2}\,, \quad I_{\rm th} = I_- \frac{v_+^2 - v_-^2}{v_+^2 - v_{\rm th}^2}\,.$$

Figure 11 presents the time evolution of the nonequilibrium distribution function obtained in the framework of the self-consistent model from the Landau equation at $\beta = 1$ and the source and sink in the form of δ-function (3.24) for a sink of intensity $I_- = -0.0001$ located at the point $v_- = 2$, and two sources located at points $v_{1+} = 1$ and $v_{2+} = 7$, respectively, with the intensities given above. It can be seen that the distribution function stays in thermodynamic equilibrium outside the inertial range, with the temperature coinciding with the initial one.

In the inertial range (corresponding to a constant energy flux between the source and sink), a distribution function that barely varies with velocity (a plateau) is set. The distribution function attains its stationary limit most rapidly in the vicinity of a source, while its formation in the vicinity of a sink takes several hundred dimensionless time units (Figs 12, 13). The increase in flux intensity (see Fig. 13) leads to the increase in the magnitude of the distribution function but leaves the temperature of the thermodynamically equilibrium distribution function without any changes.

3.3 Numerical modeling of the formation of nonequilibrium particle distribution functions for nonstationary, nonconforming sources and sinks

In the numerical simulations discussed in Section 3.2, we dealt with either sources and sinks of limited intensity or with the self-consistent model in which the sources and sinks are, first, localized in momentum space and, second, agree in intensities so as to provide a pure situation with constant energy (particle) flux in momentum space. In this case, nonequilibrium stationary distribution functions formed in the inertial range as time elapsed.

As shown in Section 4, in actual experimental practice (for example, when a solid state plasma is irradiated by a beam of high-energy ions), one is dealing not only with intensity-unmatched but also with nonstationary sources and sinks, i.e., with sources acting during a finite time interval which is much shorter than the time the sinks are active. Moreover, the sinks and sometimes the sources can be distributed over almost the entire region of momentum space. As we shall see in the subsequent exposition [29–31], the distribution functions in this case will be quasistationary or nonstationary.

Let us analyze the evolution of the distribution function for $\beta_{1,2,3} = 1, 2, 4$ under the action of only sources with low intensity. The formation of nonequilibrium distribution can be subdivided into three stages. During the first, short stage, the system still 'remembers' its initial conditions. The duration of this stage does not vary too much for different exponents β and makes approximately $t \approx 1$. The formation of the main part of the distribution happens during the second stage. Its duration essentially depends on the source position v_+, but not on its intensity, provided it is low. The distribution function acquires the shape of a plateau or gently decays between the source and the cold region, depending on the source intensity. The establishment of quasistationary distribution ends by the tail formation. Its duration depends essentially on the exponent β. The evolution of the main distribution part ends in dimensionless units for $t \approx 50$ at $\beta = 1$, for $t \approx 2$ at $\beta = 2$, and for $t \approx 1$ at $\beta = 4$.

3.4 Formation mechanism of electron distribution function for solid state plasma interacting with beams of electromagnetic radiation or fast charged particles

In this section, we intend to draw attention to specific features of conductive and emissive properties that emerge when high-energy particle beams or laser radiation act on a semiconductor plasma.

(1) Let us compare electron energy relaxation times due to electron–electron and electron–phonon collisions. Because of ionization caused by beams of intense electromagnetic radiation, electrons with energies $E \geqslant \hbar\omega$, where ω is the radiation frequency, are produced. In the case of irradiation by particle beams, the energy spectrum of released electrons embrace the interval from tens to tens of thousands of electron-volts. According to Ref. [33], the frequency of electron–electron collisions for electrons of sufficiently high energy E ($E \gg k_B T$) at high temperatures $T > T_D$ (T_D is the Debye temperature) is given by the expression

$$\gamma^{ee}(E, T) = \gamma_0^{ee}(T)\left[1 + \left(\frac{E}{k_B T}\right)^2\right], \tag{3.29}$$

where $\gamma_0^{ee}(T)$ is the classical high-temperature frequency for collisions between electrons, which is proportional to T^2. The frequency of electron–phonon collisions under the same conditions is expressed as [34]

$$\gamma^{ef} = \frac{f(T_D)\, T}{T_D}, \tag{3.30}$$

where $f(T_D)$ is the classical high-temperature frequency of collisions between electrons and phonons at $T = T_D$. For the processes discussed here, the conditions needed for formulas (3.29) and (3.30) to be valid are satisfied, since $E > 10$ eV, $T = 300$ K, and $T_D = 200 - 300$ K. Notice that quantities reciprocal to collision frequencies as given by Eqns (3.29) and (3.30) do not coincide in the general case with electron energy relaxation time, since one has to take into account the number of collisions it takes a particle to lose its energy E, i.e., the factor $\xi = E/E_1$ (E_1 is the energy lost by an electron per collision). According to data from Ref. [34], in the case considered one has

$$\gamma^{ef} \approx \gamma_0^{ee}, \quad \gamma^{ee} \gg \gamma_0^{ee}, \tag{3.31}$$

whereas the factor ξ for electron–electron collisions can be on the order of unity, while for electron–phonon collisions $E/k_B T_D > 3 \times 10^2$. Thus, the relaxation time due to electron–electron collisions is substantially shorter in this case than the relaxation time owing to electron–phonon processes.

The comparison of characteristic ionization time with the relaxation times indicates that the electron distribution function will be quasistationary in our case, and will be largely determined by the electron–electron collisions. Relatedly, it can be found from the condition that the Boltzmann (Landau–Fokker–Planck) collision integral becomes zero.

From the analysis presented above, it follows that for a semiconductor plasma in the energy interval $E - E_F > E_F$ a power-law distribution may exist, which corresponds to a constant flux of energy or particles in momentum space. In this case, the particle distribution will be formed by collisions with electrons having energies satisfying the condition $E - E_F > E_F$, as well as with (equilibrium) electrons in the basic background.

It was shown that the nonequilibrium electron distribution function is close to a universal distribution if the intensity of flux created by sources and sinks in momentum space is sufficiently large.

(2) Let us consider, as an example, the irradiation of solid state plasma by a beam of fast ions (with velocities exceeding the velocities of electrons in atoms). We concentrate on a typical situation along a track of an ion. Let the energy of a helium ion $\varepsilon_i \approx 5$ MeV, the excitation potential $\Phi \approx 100$ eV, and the ion range in matter $R_{tr} \approx 10^{-3}$ cm. Then the helium ion creates $10^4 - 10^5$ particles on its path owing to ionization, the radius of the ionization track is commensurable with the mean free path of released electrons ($R_e \approx 10^{-6}$ cm), the electron number density created by a single helium ion in its track $n_{en} \approx 10^{19} - 10^{20}$ cm^{-3}, while the equilibrium density $n_e \approx 10^{22}$ cm^{-3}. For this ratio of electron densities, the intensity of the source (sink), as can be concluded from the preceding consideration, is sufficient for the nonequilibrium distribution function to form.

We dwell on the energy loss channels for a fast ion in a solid state plasma in more detail. Notice that even for parameters characteristic of inertial thermonuclear fusion on ion beams, the interaction of ion beams with solid state plasma lacks the 'beam density effect' (cf. Ref. [35]), i.e., the dependence of ion energy loss on particle density in the beam. Bearing this circumstance in mind, we estimate the energy loss by a single ion by the Bethe–Bloch formula. According to monographs [36, 37], the energy lost by a fast nonrelativistic particle is transferred to matter in two ways. A part of the energy is spent to excite collective oscillations of the wake charge density, while the other part is transferred to individual electrons, leading to their ionization. The first part corresponds to macroscopic energy losses in distant collisions and weak momentum transfer. The second part corresponds to collisions with large transferred momenta. A relatively large part of the energy lost by the particle is spent

to excite collective oscillations. The energy $\Delta\varepsilon_k$ pertaining to the oscillations of wake charge density can be presented in the form [36, 37]

$$\frac{\Delta\varepsilon_k}{\Delta\varepsilon} = \frac{\ln(v/10v_0)}{2\ln(v/v_0)}, \quad (3.32)$$

where $\Delta\varepsilon$ is the total particle energy loss, and v_0 is the electron velocity in the ground state of a hydrogen atom. Expression (3.32) indicates that the energy $\Delta\varepsilon_k$ of wake charge density oscillations is comparable to an order of magnitude with the total particle energy transferred to the matter.

A fast particle traversing matter may create slow electrons by two equally probable mechanisms — the avalanche ionization, and the ionization through plasma oscillations. The main features intrinsic to the ionization electron formation through plasma oscillations are linked to the fairly long lifetime of wake charge oscillations, as well as to their substantial extension in space. Because of the long lifetime of the wake charge, the secondary ionization inside the beam persists long after the particle's passage. A substantial number of slow electrons in the cascade ionization are produced at the beginning of the cascade, being triggered by the secondary electron with large energy. Since the range of such an electron in matter is large, the dominant number of slow electrons are produced in cascade ionization at distances on the order of the electron range. For this reason, the ionization by the wake potential shows up as the main process that determines the distribution of ionization electrons near the axis of the particle track, while the cascade ionization governs the distribution of ionization electrons at distances on the order of the electron range from the track axis. The ionization by the field of the charged beam particle proper occurs only at the moments when the particle is flying past, while the wake oscillations of charge density play the role of the linear source of secondary electrons, which is preserved long after the passage of the charged particle and therefore markedly determine the behavior of the ionization pattern with time.

As mentioned above, despite the ion travel time along its track being small, the characteristic time of avalanche ionization by the wake charge density is rather large, reaching approximately 10^{-13} s.

If the irradiation frequency satisfies the condition $\hbar\omega \gg k_B T$, the interaction of intense electromagnetic radiation with solid state plasma results in the liberation of a large number of high-energy electrons which form, in agreement with the consideration above, the nonequilibrium stationary electron distribution function. Thus, in both cases of irradiation — by beams of intense electromagnetic radiation and by beams of fast particles — we are dealing with a nonequilibrium electron distribution function, which is formed in the inertial range as a result of electron–electron collisions described by the Boltzmann or Landau–Fokker–Planck collision integrals, and which essentially differs from the equilibrium distribution function through a large number of high-energy electrons.

4. Experimental studies of nonequilibrium particle distribution functions

Section 3.4 showed that local nonequilibrium isotropic stationary particle distributions may exist in collisional plasmas. The existence of such distribution functions hinges on the presence of sources or sinks of particles or energy in momentum space. This takes place when beams of charged particles, laser radiation, or microwave radiation interact with dense plasmas, when nuclear or thermonuclear reactions are maintained in plasma, etc. Earlier [12, 13, 15, 38], attention was drawn to a set of important consequences which, for one thing, stem from so radical a change in the energy distribution of particles and, for another, have an essential bearing on applications (influence on the Landau damping, the Lawson criterion in tasks of controlled fusion, application in astrophysics, and others). However, gas plasma constitutes a highly unstable medium in which collective processes may play a particularly important role and 'conceal' the collision phenomena between particles. From this viewpoint, solid state plasma, allowing one to control the departure from equilibrium in a stable regime, seems to be more attractive. Here, the source or sink of energy (particles) can be furnished by ion beams, powerful laser radiation, an emission current, beams of charged particles produced in fusion or fission reactions, and so forth.

In this section, our goal is to draw attention to specific features of conductive and emissive properties of metals and semiconductors subject to the action of intense beams of particles or laser radiation. In this connection, Sections 4 and 5 consider anomalies in the emissive properties of metals, enabling one to create new sources of current or converters of the radiation energy into electric energy, promising substantial advantages over thermionic ones (see, for example, Ref. [39]) with respect to their efficiency and emission current [16].

4.1 Experimental studies of nonequilibrium electron distribution functions in emission induced by laser radiation

Paper [12] called attention to the possibility of an anomalous increase in the photoconductivity of a semiconductor exposed to light of frequency ω insufficient to trigger the transition between its bands, $\hbar\omega < V_g$, where V_g is the band gap width, by creating a nonequilibrium distribution of electrons and holes. Based on experimental research, the authors of Ref. [40] pointed to the significant modification of the conductive properties of semiconductors irradiated by α-particles.

It is known [41, 42] that two peaks in the emission current are observed on illuminating metal foils by a nanosecond pulse of a powerful laser, $Q = 10^{14}$ erg $(\text{cm}^2\,\text{s})^{-1}$. The first peak, almost synchronous with the laser pulse, contains a large number of 'fast electrons' (the maximum energy for tungsten is 14.5 eV). The second peak, lagging $\tau \sim 10^{-7}$–10^{-8} s behind the first one, contains electrons with energies that do not exceed 2 eV. A satisfactory explanation for the appearance of fast electrons as being due to the Maxwell distribution function is impossible [43], because the experimental results of Refs [41, 42] would correspond to the temperature $T_e = 30{,}000$ K, which is an order of magnitude higher than the tungsten melting temperature. As concerns the emission current, two mechanisms of its production are well known: the multiquantum photoeffect and thermionic emission, both giving emission currents which are smaller by many orders of magnitude.

Turning to the mechanism based on a nonequilibrium electron distribution function forming under these conditions [13, 38], one gets plausible estimates for the magnitude of emission current and its dependence (fast peak) on the retarding potential. As for the slow peak, in all probability,

over its initial part the emission current is contributed not only by the equilibrium distribution (thermionic emission) but also by a nonequilibrium nonstationary component linked to the 'breakup' of power-law distribution.

If the intensity of laser beams is very large, a plasma layer builds up near the solid body surface, and the appearance of high-energy electrons may be explained by a soliton formation under resonance pumping [44]. This mechanism, however, has only a limited validity domain and is unsuitable for explaining the experimental results obtained by Knecht [41, 42].

Thus, it is shown that a series of experimental data on the magnitude of emission current from metals, induced by laser irradiation, and the dependence of current on the retarding potential [41, 42] cannot be explained in the framework of equilibrium distribution function [43], but gains a satisfactory explanation with the help of mechanism [13, 38] that hinges on the presence of a nonequilibrium situation.

4.2 Experimental studies of nonequilibrium electron distribution functions in emission induced by beams of fast ions

To describe kinetic electron emission induced by ions, one resorts to theories proposed in Ref. [45] for low ion energies, and in Ref. [46] for the range of high energies. According to the mechanism of secondary emission proposed by Sternglass [46], secondary electrons are formed because of ionization by fast ions, as described by the Bohr–Bethe theory, then diffuse to the surface and exit into a vacuum. The secondary emission coefficient Δ_e for this mechanism is proportional to the specific ionization losses and does not depend on the work function φ, conductivity, or other basic properties of the substance. Notice that, for the thermal mechanism of emission, the coefficient Δ_e is proportional to the square of specific ionization losses and essentially (exponentially) depends on the electron work function.

In reviews and experimental studies [47–75] and in the literature cited therein, it is proven that the secondary emission coefficient Δ_e is proportional to the energy loss by fast particles, i.e., available data confirm the mechanism described in Ref. [46]. It is noteworthy that the proportionality coefficient κ in this dependence is practically independent of the incident ion energy, but depends on the target material and may change severalfold if one material is replaced by another. Prior to research involving nonequilibrium particle distributions, both theoretical and empirical expressions linking the proportionality coefficient κ with the target parameters and incident ion energy were absent.

Theoretical consideration of secondary electron emission from aluminum, induced by protons and α particles and carried out in Refs [65, 75, 76], is not able to predict the values of coefficient κ observed experimentally or explain the broad energy spectrum (especially for forward emission) of secondary electrons. Note that most experimental research is concerned with backward emission. However, as shown in Ref. [54], the energy spectrum of secondary (backward) electrons is not universal if the energy of the impinging particle is varied. In this case, even such a rough characteristic of the process as the ratio of the forward secondary emission coefficient to the backward one may vary (see Refs [54, 70]).

In our opinion, the expression for the secondary electron emission coefficient Δ_e that is most physically transparent is offered by the formulas

$$\Delta_e = \kappa \frac{d\varepsilon}{dx}, \quad \kappa = \frac{PL_e}{\varepsilon_e}, \tag{4.1}$$

proposed in accordance with Refs [46] and [59] and used in Ref. [55], where $d\varepsilon/dx$ is the energy loss by an impinging particle, P is the probability of the event that the surface barrier will be surmounted by an internal secondary electron, L_e is the depth of the layer from which the emission electrons emerge, and ε_e is the energy spent for every internal secondary electron formation. Reference [59] suggests taking ε_e equal to that of the respective substance, but in a gaseous phase under normal conditions.

We suppose that the secondary emission coefficient Δ_e should be proportional to the energy loss per atom, i.e., be dependent on the number density of atoms N_a as $N_a^{-1/3}$, and be inversely proportional to the excitation potential Φ taking into account the collective character of the interaction of a charged particle with the electron subsystem of the target material. In accordance with Refs [77–79], the Sternglass formula is modified as follows:

$$\Delta_e = \frac{\zeta Z_{1\text{eff}}^2}{\Phi N_a^{1/3}} \left(-\frac{d\varepsilon}{dx}\right)_p, \tag{4.2}$$

where $(-d\varepsilon/dx)_p$ is the energy loss by a proton moving with the velocity of the impinging ion, $Z_{1\text{eff}}$ is the effective ion charge in the target, and ζ is some constant. In this case, it is reasonable to use an expression for $(-d\varepsilon/dx)_p$ proposed in Ref. [80] and valid in the beam energy range from several keV to 50 MeV:

$$\left(-\frac{d\varepsilon}{dx}\right)_p = \frac{ay + by^2}{0.01y^{2.55} + c_1}, \tag{4.3}$$

where y is the velocity ($\times 10^8$ cm s^{-1}), and a, b, c_1 are coefficients characterizing the material of the target and having a rather pronounced periodic dependence on the atomic number Z_2 of the target element. Thus, the coefficient a varies with a period close to $Z_2 = 18$. The values of coefficients a, b, and c_1 for aluminum, beryllium, graphite, and nickel [80], which are used in Section 4.3, are collected in Table 3.

The energy dependence of secondary emission coefficient Δ_e is explored rather thoroughly, yet the description of the distribution of emitted electron over energies emerges as a rather tough problem. Results of experimental research on the energy spectrum of secondary electrons emitted when protons or α particles traverse thin foils are reported in Refs [47–79, 81–84]. However, in Refs [81–83] the spectrum was explored in a narrow energy range (0–10 eV), and it is only mentioned that the spectrum is of a nonthermal nature, and in Refs [54, 55, 79], although their measurements cover a

Table 3. Coefficients characterizing the target material.

Material	a	b	c_1
Al	2.4	0.018	0.36
Be	2.42	0.001	0.37
Ci	2.92	0.018	0.4
Ni	6.8	0.01	0.77

wide secondary-electron energy range (0–100 eV), the distribution function can be judged only by its integral characteristic because of imperfections in the experimental technique utilizing a nonspherical analyzer, which is not fully satisfactory. Reference [54] proved that for a broad range of proton energies (20–250 keV) the energy spectrum of secondary electrons in the forward direction is defined by a universal power-law function, whereas for the backward emission such a universal dependence is absent. Additionally, it was shown that the forward secondary emission coefficient is almost twice as large as the backward one. It can readily be seen that, by studying the energy spectrum of secondary electron emission (SEE) with a spherical analyzer for a point source of SEE, it is possible to retrieve the electron distribution function in a metal. The emission current is determined as

$$I_{\mathrm{em}} = B_1 \int_{\varphi+E_{\mathrm{F}}+q_{\mathrm{e}}U}^{E_{\max}} Ef(E)\,\mathrm{d}E\,, \tag{4.4}$$

where U is the retarding potential, and B_1 is a constant; therefore, the derivative of current over the retarding potential is proportional to the electron distribution function:

$$\frac{\mathrm{d}I_{\mathrm{em}}}{\mathrm{d}U} = B_2(\varphi + E_{\mathrm{F}} + q_{\mathrm{e}}U)f(\varphi + E_{\mathrm{F}} + q_{\mathrm{e}}U)\,. \tag{4.5}$$

When the electron distribution function has a power-law form, plotting the dependence of $\mathrm{d}I_{\mathrm{em}}/\mathrm{d}U$ on $\varphi + E_{\mathrm{F}} + q_{\mathrm{e}}U$ in logarithmic coordinates enables one to easily find the power-law exponent from the slope of the curve.

To verify the theoretical ideas pertaining to the mechanism of electron distribution function formation in interactions of ion beams with a solid state plasma, formulated in Sections 2 and 3, an analysis was carried out of the experimental secondary electron energy spectrum and the dependence of the secondary emission coefficient Λ_{e} in the forward direction, not only on energy losses of α particles and protons in matter, but also on the excitation potential Φ.

The comparison of current–voltage characteristics for different targets with due account of thermal electrons invites the conclusion that the mechanism of secondary emission is not thermal and that secondary electrons knocked out the target by α particles are distributed according to a law different from the exponential one.

4.2.1 Study of kinetic electron emission from metals. We turn now to presenting experimental results on the exploration of the secondary electron energy spectrum with the aid of a spherical three-grid analyzer. Such measurements allow one to retrieve the power-law exponent s of the electron energy distribution function with the help of a single differentiation of the current–voltage characteristic because, in this case, in the domain where the distribution function follows the power law, we have

$$\frac{\mathrm{d}I_{\mathrm{em}}}{\mathrm{d}U} = B_3(\varphi + E_{\mathrm{F}} + q_{\mathrm{e}}U)^{s+1}\,, \tag{4.6}$$

where B_3 is a constant.

Accordingly, dependence (4.6) is a straight line on the logarithmic scale with the tangent of the slope angle equal to $s+1$.

The experimental points for the dependences of $\lg(\Delta I_{\mathrm{em}}/\Delta U)$ on $\lg(\varphi + E_{\mathrm{F}} + q_{\mathrm{e}}U)$ for aluminum and beryllium targets are well fit by three straight lines, which corresponds to different power-law exponents in the energy intervals 0–10 eV, 10–40 eV, and 40–100 eV. The exponents s for aluminum and beryllium are only different in the range of small energies.

Departing from expression (4.3) for the particle energy loss, and taking into account the values of coefficients a, b, and c, it is possible to explain the dependence of secondary emission coefficient Λ_{e} for aluminum and nickel on the energy ε of impinging particle in the form $\Lambda_{\mathrm{e}} \sim \varepsilon^{-0.73}$ in a wide energy range, which was mentioned in Refs [64, 65]. Since $\Phi\,[\mathrm{eV}] \approx 13.5Z_2$ [85, 86], in the energy interval from 1 to 10 MeV the range of an α particle in matter is determined from the empirical formula [86, 87]

$$R_{\mathrm{tr}} = 0.174 \times 10^{-3} A_{\mathrm{m}}^{1/3} \rho_{\mathrm{m}}^{-1} \varepsilon^{3/2}\,, \tag{4.7}$$

where A_{m} and ρ_{m} are the atomic weight and the density of matter, respectively. For estimates, it can approximately be assumed that

$$\Lambda_{\mathrm{e}} \sim Z_{\mathrm{leff}}^2 \frac{\rho_{\mathrm{m}}^{2/3}}{Z_2} V_{\mathrm{b}}^{-1}\,, \tag{4.8}$$

where V_{b} is the velocity of impinging particle. Formulas (4.7) and (4.8) provide the correct relationship between the secondary emission coefficient Λ_{e} for aluminum, beryllium, and graphite. High absolute values of Λ_{e} obtained in Refs [77, 79] are explained by a substantial contribution to the electron emission from α particles flying at an angle to the normal to the film and experiencing higher energy losses than the particles moving in the direction of the normal.

In order to alleviate the drawback of Ref. [79] caused by averaging the secondary electron spectrum over energies of impinging particles and the take-off angle of the secondary electrons, the experimental research dealing with the energy spectra of secondary electron emission induced by a proton beam traversing a target was carried out for different electron take-off angles for Al, Cu, and Be [78, 88]. The dependence of secondary emission coefficient in the forward direction was studied not only with respect to the energy loss of protons with an energy of 1 MeV in matter, but also to other macroscopic characteristics of the target. The energies of secondary electrons knocked out of the target were analyzed by the retarding potential method with the aid of a narrow-aperture (4×10^{-4} steradian), three-grid analyzer mounted at different angles (30°, 45°, and 75°) to the beam direction. The secondary emission coefficient was determined by the ratio of the total secondary electron current I_{e} to the current of protons I_{p}. The experiments utilized targets with a thickness of 5.6 μm for aluminum, 9.7 μm for beryllium, and 1.2 μm for copper. The measured dependences of $I_{\mathrm{e}}/I_{\mathrm{p}}$ on U allow one to determine the power-law exponent s by once differentiating these dependences because, in this case, in the range where the distribution function follows the power law, we have

$$\frac{\mathrm{d}}{\mathrm{d}U}\frac{I_{\mathrm{e}}}{I_{\mathrm{p}}} = B_4(\varphi + E_{\mathrm{F}} + q_{\mathrm{e}}U)^{s+1}\,, \tag{4.9}$$

where B_4 is a constant.

Consequently, function (4.9) represents a straight line on the logarithmic axes, the tangent of its slope being $s+1$. It was shown that the experimental points gather around three straight lines that correspond to different power-law exponents on the intervals 0–10 eV, 10–40 eV, and 40–100 eV.

These exponents coincide rather accurately ($\sim 10\,\%$) with those found with the aid of a spherical analyzer in the experiments on bombarding the same targets by α particles (see above and Ref. [77]). The power-law exponents were found to differ for different targets only in the range of small energies 0–10 eV. Together with the energy spectrum, the values of the integral characteristic — the secondary emission coefficient Δ_e for aluminum, copper, and beryllium targets — were determined to be equal to 2.5, 1.6, and 4.6, respectively. As we have already mentioned, the coefficient Δ_e is proportional to the energy loss of a fast particle:

$$\Delta_e = \kappa \frac{d\varepsilon}{dx}, \tag{4.10}$$

where κ is the proportionality coefficient, which may vary several times between various materials.

The experimental results for the three targets considered here agree with the data for aluminum and beryllium discussed earlier and the data of Ref. [70] for graphite. The coefficients Δ_e for different targets relate as the reciprocal of the excitation potential Φ multiplied by $N_a^{1/3}$. We note that the data for copper [88] are somewhat worse, but, possibly, this stems from the imperfect character of the surface layer for the copper foil used.

Thus, the experimental studies of the energy spectrum of secondary electrons demonstrated that the electron energy distribution function is essentially nonequilibrium and decays by a power law as energy is increased, with the same exponents for energies in excess 10 eV for different target materials. They confirmed the proposed theoretical dependence of the secondary emission coefficient on the excitation potential Φ and the number density of atoms N_a.

Electron distributions over energies have been studied in the case of ion–electron emission induced by beams of H^+ ions with energies from 0.75 to 3.0 MeV, and H_2^+ ions with energies from 1 to 2.5 MeV. The ion beam current comprised 0.1–0.4 μA, while the beam diameter on target was 3 mm in all experiments. Thin foils made of silver, copper, nickel, or titanium were used as targets, and their thickness was less than the range of H^+ and H_2^+ ions with the given energy in the target material. The residual gas pressure in the vacuum camera reached 10^{-6} Torr. The energy distributions of secondary electrons were measured in a spherical analyzer with a retarding field. The latter was created between the target and two hemispheres. To eliminate the electron emission under the action of a stream of striking particles, the Faraday cylinder was under the antidynatron potential (~ 20 V) created by a DC power source. The current of the Faraday cylinder was amplified by an electrometric amplifier. The signal from the amplifier was passed to a D3-28 computer. The current of electrons overcoming the retarding field of the analyzer was collected by a forward hemisphere and, after amplification, passed to the computer, too. The emission current I_e of secondary electrons was measured on two intervals of electron energy U: 5–50 eV with a step of 1 eV, and 35–200 eV with a step of 5 eV. The operations of preliminary processing were performed automatically with the assistance of specially developed software. Expression (4.6) was rewritten in the form

$$y = (s+1)\,x + a, \tag{4.11}$$

where $y = \lg(dI_e/dU)$, $x = \lg(U + E_F + \varphi)$, and $a = \lg B_3$, and then the exponent s and parameter a were determined.

Table 4. Absolute values of power-law exponent s as a function of proton energy.

E_p, MeV	Titanium	Nickel	Copper	Silver
0.75	5.4 2.28	5.6 1.88	7.74 1.81	6.54 2.7
1.0	5.15 2.0	4.66 1.45	6.36 1.64	6.52 2.54
1.5	5.95 2.64	5.38 2.32	5.8 0.86	6.42 1.98
2.0	7.16 2.93	5.53 2.78	5.77 2.85	4.38 2.08
2.5	6.06 2.12	4.58 1.64	5.01 2.11	5.25 1.96
3.0	5.66 1.88	4.32 1.66	5.73 2.67	6.34 2.7

Table 5. Absolute values of power-law exponents s as a function of the H_2^+ ion energy.

$E_{H_2^+}$, MeV	Titanium	Nickel	Copper	Silver
1.0	6.04 1.98	5.34 1.87	2.81 2.43	
1.5	4.66 1.82	3.40 1.18	5.36 2.36	6.73 2.0
2.0	4.56 1.49	4.09 1.57	3.66 2.16	6.11 2.54
2.5	4.31 1.28	8.73 2.62	5.73 2.67	5.48 2.7

The fit skill was characterized by the parameter

$$q_{fit} = \frac{1}{N_y} \sum_{i=1}^{N} \left(1 - \frac{y_{exp}}{y_{theor}}\right)^2. \tag{4.12}$$

Here, N_y is the number of y values used in determining the exponent s:

$$y_{exp} = \lg\left(\frac{1}{U}\frac{dI}{dU}\right), \quad y_{theor} = \lg\left(\frac{1}{U}\frac{dI_{theor}}{dU}\right), \tag{4.13}$$

where the function dI_{theor}/dU is computed by formula (4.6) using the values of s and B_3 found.

Typical plots of the secondary electron spectrum were approximated by two straight lines on the intervals from 5 to 30 eV, and from 30 to 250 eV, with different values for the power-law exponent.

Table 4 lists the values of power-law exponent s for the two regions (the upper and lower values) as a function of the energy of the impinging beam of H^+ ions for different target materials. Table 5 displays the same quantities, but for a beam of H_2^+ ions.

As can be seen from Tables 4 and 5, in most experiments the power-law exponent in the first region (upper values) increases together with the ion energy loss in the matter. In the second region (lower values), an apparent dependence escapes detection.

4.2 2 Studies of kinetic electron emission from semiconductors. The information available in the literature on emissive properties of materials irradiated by beams of fast ions largely pertains to metals. The apparent lack of data for effective electron emitters widely used in photoemission and

electronic devices cannot escape attention. The effective secondary electron emitters based on antimony and cesium compounds are disseminated most widely. Owing to their high secondary photoemission and electron emission coefficients, which are commonly attributed to low heights of the potential barrier at the interface between the sample surface and a vacuum, materials of that type are actively used as photocathodes and dynodes in photoelectron multipliers and other devices [89, 90]. Indeed, the value of the secondary electron emission coefficient for antimony–cesium cathodes ranges $\Delta_e = 3-4$ for a low energy of primary electrons $E_e = 100$ eV, and the maximum value amounting to $\Delta_{e\,max} = 8-10$ for the SEE coefficient is achieved at energies $E_e = 500-600$ eV [89, 90]. The rather high secondary emission coefficient is the consequence of not only the low work function for this material but, arguably, also the formation of nonequilibrium distribution functions of the power-law form.

The study of the distribution functions of electrons formed in the solid state plasma of an antimony–cesium cathode hit by beams of fast light ions was carried out on a setup described in detail in Ref. [32]. An electrostatic Van de Graaff ion accelerator, used as a source of primary particles, made it possible to produce beams of hydrogen (H^+) and helium (He^+) ions. Measurements of the energy spectra of electrons of secondary ion–electron emission (SIEE) were carried out for beams of H^+ ions with energies from 1.00 to 2.25 MeV, and He^+ with energies from 1.75 to 2.25 MeV with a step of 0.25 MeV. The explored cathode, utilized as a target, consisted of an antimony-cesium layer with a thickness exceeding the range of impinging ions in the material, fitted to a massive nickel substrate. The target 10 mm in diameter was fixed in a copper casing attached to a moving holder. The ion beam collimated with the aid of a system of diaphragms hit the target causing SIEE from its surface in the backward direction. The plane of the target was installed perpendicularly to the beam axis. The beam diameter on the target measured 3 mm. The ion current density at the target did not exceed 30 μA cm^{-2}. The chamber was pumped out with an NMD-0,4-1 magnetic-discharge pump and NVPR-16D forevacuum pump with a nitrogen trap. In all experiments conducted, the residual vacuum in the chamber was at least 10^{-6} Torr. Electrons emitted from the target surface were collected at a spherical collector made of two hemispheres of radius 100 mm. The target on the holder was placed inside the collector. The gap between the hemispheres equaled 15 mm. The entrance window of each hemisphere was 10 mm in diameter. Simultaneously with the collector current I_C, the target current I_T was measured, too. The target current represents the sum of the ion beam current I_B and the current of secondary electrons that reached the collector: $I_T = |I_C| + I_B$. The measured currents of collector I_C and target I_T, amplified by electrometric amplifiers, were passed to a personal computer via an analog-to-digital converter. To calibrate the measuring system, the Faraday cylinder was located behind the rear hemisphere, enabling direct registration of the ion beam current I_{FC} when the beam was not traversing the target. The Faraday cylinder was 20 mm in diameter and had the length $l = 130$ mm. The Faraday cylinder current I_{FC} was measured with the help of an F303 current instrument. The SIEE coefficient was determined from the formula

$$\Delta_{ie} = \frac{|I_C|}{|I_C| - I_T}\,. \tag{4.14}$$

Studying the energy spectrum of electrons produced by SIEE with the aid of a spherical analyzer for a pointwise emission source, one can reconstruct the explicit shape of the electron distribution function inside the solid substance [16, 32, 78]. When the distribution function exhibits a power-law shape, the derivative of the emission current over electron energy, dI/dU, can be written out as

$$\frac{dI}{dU} = B(E_F + \varphi + eU)^{s+1}\,, \tag{4.15}$$

where B is a constant. Consequently, on the logarithmic axes, dependence (4.15) represents a straight line inclined at an angle with tangent equal to $s + 1$.

The energy distributions of secondary electrons in backward emission were measured with the help of a spherical collector in the energy analyzer mode with a retarding field on the interval from 0 to 100 V with a step of 1 V. The retarding electric field was created between the target and the two hemispheres. Since the radius of the energy analyzer was substantially larger than the target size, the field configuration was close to a spherically symmetric one. A ceramic tube covered from the outside with a resistive layer and measuring 5 mm in diameter was used as the target holder. The resistivity of the layer R_l was varied nonlinearly along the tube so that the holder potential did not disturb the field inside the analyzer. The target had a galvanic contact with one end of the resistive layer, while its other end was grounded. The retarding potential was fed to the target inside the ceramic tube from a source of saw-tooth voltage controlled through a PC. Accordingly, the current flowing along the resistive layer created the required potential distribution along the length of the holder. In the experiment, secondary electrons reached the collector while moving radially. When the retarding potential was applied to the target, only electrons with energies sufficient to overcome the retarding field reached the collector. The software controling the experiment enabled collecting statistics of 100 measurements of the electron emission current during 7 s for every magnitude of retarding potential. It then carried averaging over these 100 experimental points, writing the result to computer memory. Differentiating the measured dependences of the collector current on the retarding potential (the retardation curves), one may retrieve the energy spectrum of SIEE electrons and then reconstruct their distribution function.

The experimental research of the energy spectrum of SIEE electrons carried out in this manner indicates that, for all explored energies of ions, the electron distribution function formed under nonequilibrium conditions in the plasma of antimony–cesium cathode has a power-law shape.

Figure 14 displays a typical distribution function for nonequilibrium electrons for the explored sample hit by He^+ ions with an energy of 1.75 MeV.

The experimental points are well fit by two straight lines corresponding to different power-law exponents in the energy ranges 5–30 eV and 30–100 eV. By processing the experimental data, the respective exponents were recovered. Table 6 lists the values of exponents $-s_{E1}$ and $-s_{E2}$ for the two portions of the distribution function, which correspond to the energy intervals specified above, as a function of the energy of impinging H^+ and He^+ ions.

In our opinion, the power-law exponent of the secondary electron distribution function may preserve generally the dependence on the energy (specific ionization losses) of fast ions, since the intensity of the source of additional particles in

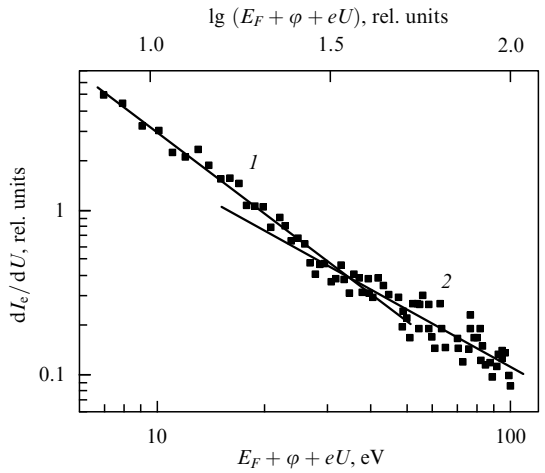

Figure 14. Typical dependence of $\lg(dI_e/dU)$ on $\lg(E_F + \varphi + eU)$ for an antimony–cesium cathode bombarded by He^+ ions with the energy of 1.75 MeV. Section *1* of the distribution function (the energy range 5–30 eV) is described by the power-law with exponent $s_{E1} = -2.9$, and section *2* (30–100 eV) with $s_{E2} = -2.5$.

Table 6.

Ion	Energy, MeV	$-s_{E1}$	$-s_{E2}$
H^+	1.25	2.9	2.5
	1.5	3.0	2.5
	1.75	2.9	2.5
	2.0	3.0	2.4
	2.26	3.0	2.6
He^+	1.75	2.9	2.5
	2.0	2.8	2.2
	2.26	2.8	2.3

momentum space is defined precisely by the ion's specific ionization losses. As was pointed out in Refs [13, 16, 17], the power-law exponent is independent of the structure of sources and sinks only under certain special conditions. In such cases, one speaks about the universal electron distribution function with the exponent $-5/4$ [16]. In experiments conducted earlier with the He^+ ion beam and thin metallic films, the exponents s were measured, and it was shown that the absolute value of power-law exponent s_{E1} of the distribution function on the first energy interval, corresponding to the range of slow electrons ($E < 35$ eV), decreases with the growth of the ion's specific ionization losses in metals [91]. The authors of Ref. [57] point out that a fraction of the fast electrons increases together with the energy of impinging ions. As is seen from Table 6, the exponents s_{E1} differ but slightly for different energies of impinging ions and, consequently, for different specific ionization losses of ions in an antimony–cesium sample, although the absolute value of the power-law exponent grows (decays) for protons with an increase in energy (specific ionization losses). Such behavior is not observed for helium ions. Noteworthy is the fact that the variation of the power-law exponent is within 10%, so that additional research is needed to reliably establish its dependence on energy losses.

Figure 15 plots the dependence of electron emission yield Δ_e on the energy of incident H^+ and He^+ ions for the antimony–cesium cathode. As can be concluded from the plot, the values of electron emission yield Δ_e for the explored

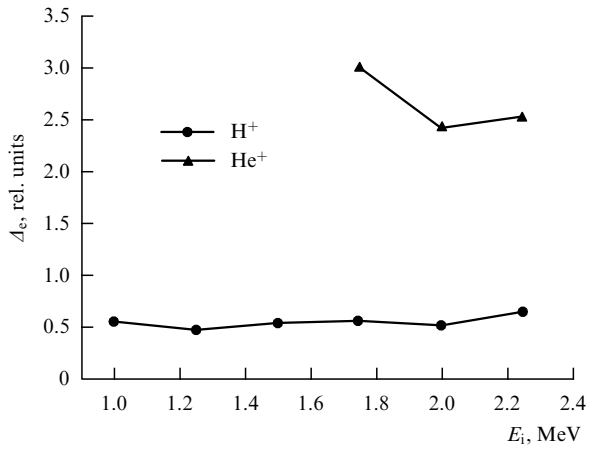

Figure 15. Dependence of electron emission yield Δ_e on the energy of impinging H^+ and He^+ ions for an antimony–cesium cathode.

antimony–cesium compound exceed those for many metallic samples [59]. This may have the following cause. As has already been mentioned, a part of the nonequilibrium electrons, formed in a solid state plasma bombarded by beams of fast charged particles, diffuses to the surface and are ejected into the vacuum. The electron emission occurs from a subsurface layer substantially thinner than the ion penetration depth and is governed by laws defining the motion of these electrons to the surface.

The results of experimental studies presented in Ref. [32] also point to the dependence of the electron emission yield Δ_e induced by He^+ ions from a germanium sample on specific ionization losses dE/dx of He^+ ions, which is approximated well by a straight line, thus confirming the proportionality between these quantities. It should be mentioned that ion beam currents considered in Ref. [32] do not exceed 10 μA. In this case, the emission current varies noticeably with time, reflecting the nonstationary behavior of sources and sinks in energy space. For every ion track, the electron distribution function has sufficient time to pass all stages of its evolution, so that the dependence of emission current on the retarding potential observed in the experiments stemmed from the superposition of currents produced during all time intervals when the nonequilibrium electron distribution function existed. Figure 16 presents the dependence of emission current on retarding potential [29–32]. The main result of comparing theoretical and experimental data is the conclusion that the account for source nonstationarity is an essential factor in explaining the dependence of current on retarding potential, when the experimental technique of collecting the charge escaping the entire film surface over a sufficiently long time interval (several seconds) is utilized. Figure 17 compares electron number densities $N(E) \sim f(v, t)\, v$ for nonstationary electron distribution functions simulated numerically at various time instants [30, 31] with those observed in the experiment [84] for secondary emission electrons induced by 1-keV electrons from polycrystalline aluminum (A1). The energy of the volume plasmon amounts to 15.5 eV, and the A1 work function equals 5.25 eV [31, 84].

4.3 Direct transformation of particle kinetic energy into electric energy based on nonequilibrium particle distributions

Based on the research findings discussed in Sections 4.1 and 4.2, a secondary-emission radioisotope current source has

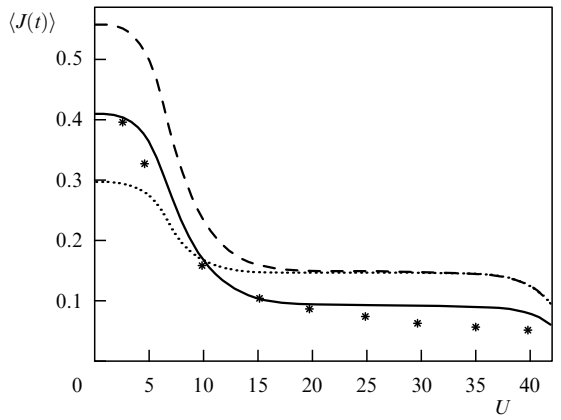

Figure 16. Dependence of ion–electron emission current on the retarding potential for gallium arsenide (GaAs) bombarded by H^+ ions with an energy of 1.25 MeV. The curves correspond to the current averaged over time $t = 10$ (dotted line), 20 (dashed line), and 100 (solid line); the stars display the experimental results [32].

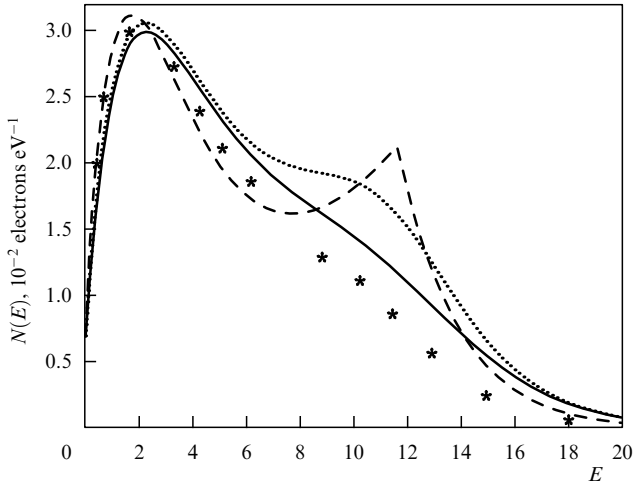

Figure 17. Dependence of the number density of electrons with energy E, $N(E) = f(v)\,v$, on the energy of emission electrons produced by 1-keV electrons bombarding polycrystalline aluminum. The solid, dashed, and dotted curves correspond to the results of numerical modeling, and the stars plot the experimental data [84].

been developed [92–100], containing a radioisotope layer in a hermetic enclosure under conditions of sufficiently high vacuum. This layer was sandwiched between metal emitters whose thickness does not exceed the range of charged particles emitted by the radioisotope in the respective metal. Each of the emitters is fabricated as a sequence of alternating layers of two distinct metals with different secondary electron emission coefficients, insulated electrically by vacuum gaps. The efficiency of a radioisotope source of this type is determined by the fact that secondary electrons are produced along the entire path of a charged particle in metals, i.e., the energy of charged particle is directly converted into the energy of electrons, the number and mean energy of which are incommensurately higher than in the thermionic emission. It was established that making use of heavy particles in sources of electric current leads to a high secondary electron emission coefficient owing to a negligibly small scattering of these particles, since their motion is approximately rectilinear. The secondary electron distribution function is nonequilibrium, with the mean energy of emitted electrons exceeding 10 eV. The source efficiency coefficient increases as a result of augmented secondary emission under the action of δ-electrons (see Refs [95–97]). This source, therefore, has high energy indices which are directly proportional to the number of emitter layers. Since the full thickness of the emitter does not exceed the range of a charged particle emitted by the radioisotope, the increase in layer number, and hence emitter efficiency, is only possible by making layers thinner. However, with a reduction in thickness the layers lose their constructive rigidity, and as a result their electric isolation may be destroyed, for example, because of sagging when the vacuum gap between the layers gets thinner. Subsequently, a secondary emission source of current possessing sufficient constructive rigidity for layers of reduced thickness was offered [98–100]. Its emitter consists of alternating, electrically isolated layers of two unlike materials with different secondary electron emission coefficients. The emitter layers are separated by dielectric grids which electrically insulate the layers and increase the stiffness of the emitter's construction. In so doing, the dielectric grids are thicker than the working layers of the emitter. To achieve the best results when implementing this invention, the grid from a dielectric material (ceramic or plastic) should be superimposed directly on one of the emitter layers. To boost the energy efficiency of the proposed current source, it is desirable to make one of the alternating layers in the emitter from a metal, and the other one from a semiconductor material with a higher secondary electron emission coefficient than for the metal of the first layer.

5. Kinetics of an electron–phonon system of a crystal in a strong electric field

In the 1960s, the phenomenon of a sharp reduction in the plastic resistance of metals was discovered, whereby the conduction electron subsystem of metals is excited either by irradiating them by fast charged particles or by passing high-density electric current $j = 10^8 - 10^9$ A m^{-2}. It could not be reduced to a trivial thermal action (in a macroscopic manifestation) of current, so an assumption has been put forward on the existence of electron–dislocation interaction influencing the mechanical properties of crystals [101, 102].

It was proposed to call the phenomenon the electroplastic effect (EPE). The mechanism of the EPE was associated with an increase in mobility of dislocations in the domain with sources and, hence, with the intensification of source operation. In its purest form, the EPE was explored in metallic single crystals of Zn, Cd, Sn, and Pb [101]. If samples of these materials in a process of deformation are subject to current pulses $10^2 - 10^3$ A mm^{-2} in magnitude and 10^{-4} s in duration or are irradiated with accelerated electrons in the slip direction, a reduction in strength is observed, manifested in a jumplike drop in deforming stress. Oscillations of stress are linked to jumps in the plastic strain of objects. It was discovered that, synchronously with the passage of current pulses and the reduction in the deforming force, groups of slip bands are formed, and also that the jumps in deforming force are much smaller in the range of quasielastic deformations than after the yield point. These oscillations are anomalously high in the vicinity of the material yield point. Jumps in deforming force in diagrams decrease in tests carried out in the stress relaxation mode. A characteristic feature of the EPE in single crystals is the absence of temperature dependence in a broad interval from 77 to 300 K.

It was shown that as the electron energy is increased past the knock-out threshold for atoms ($E_{tr} \approx 0.7$ MeV for zinc), the augmented plasticity of a metal on irradiation is overlain by the effect of its hardening on irradiation, caused by the appearance of additional stoppers for dislocations in the form of point defects and their ensembles. If the electron density in a pulse is increased, the plasticity on irradiation first increases and then weakens. Weakening of the effect is explained by the influence of possible partial degeneration of electron gas in a metal on motion and interaction of dislocations [102].

It is shown that the activation volume does not change considerably on irradiation of a metal by electrons and that an increase in creep rate is explained by the decrease in the time scale (increase in the frequency) of the process of thermally activated passage of barriers by dislocations [102].

5.1 Kinetic description of the electroplastic deformation effect

The plastic deformation of crystals under applying an external load occurs in most cases through dislocation slip [103]. The pertinent basic equation (the Orowan relationship) governing the kinetics of plastic deformation in a slip plain has the form

$$\dot{\mathcal{E}}_d = b\rho_d V_d(\sigma^*, T)\,, \tag{5.1}$$

where $\dot{\mathcal{E}}_d$ is the plastic deformation rate, ρ_d is the density of mobile dislocations, b is the magnitude of their Burgers vector, and $V_d(\sigma^*, T)$ is the mean velocity of long-range dislocation displacement, which depends on the effective deforming shear stress $\sigma^* = \sigma - \sigma_i$ and the temperature T, where σ_i are the internal shear stresses in the slip plane (the analog of dry friction). In the region of sufficiently weak σ^*, a moving dislocation colliding with local stoppers (impurity atoms or other defects of a crystalline lattice) may linger there over a long time. It is believed that the mechanism by which a dislocation segment surmounts barriers involves thermal fluctuations, provided temperatures are not too low. Then, one has

$$V_d(\sigma^*, T) = lv(\sigma^*, T) = lv_0 \exp\left(-\frac{H(\sigma^*)}{k_B T}\right), \tag{5.2}$$

where l is the mean distance between stoppers, and $v(\sigma^*, T)$ is the frequency they are passed through. The explicit form of function $H(\sigma^*)$ depends on the model of the potential barrier (its amplitude and shape) retarding the dislocation slipping, and also on the barrier distribution along the dislocation line. In experimental data processing, it is routinely assumed that

$$H(\sigma^*) = H_0\left(1 - \left(\frac{\sigma^*}{\sigma_{cr}}\right)^{p_0}\right)^{q_0}. \tag{5.3}$$

If the role of stoppers is played by impurity atoms, then H_0 is the energy parameter of dislocation–impurity interaction, σ_{cr} is the critical stress for dislocation motion through a grid of impurity barriers in the slip plane without activation, and p_0, q_0 are some power-law increments determined from the analysis of experimental curves.

5.2 Mathematical model

To quantitatively describe the dynamics of an electron–phonon system in a metallic film, Ref. [104] resorted to an important simplifying assumption that the isotropic part of the electron distribution function is a Fermi type with a time-dependent electron temperature. The authors of Ref. [104] note that, although the introduction of electron temperature is equivalent to a frequently used assumption on instantaneous thermalization of an electron subsystem, it cannot always be strictly justified. So, in the region of very low temperatures $T_e < T^*$ (the temperature $T^* \approx T_D^2/E_F$), where electron–electron collisions dominate electron–phonon collisions, the electron distribution function is thermalized on the time scale of electron–electron interaction, τ_{ee}. In ordinary, relatively pure metals, $T^* \sim 1$ K, while in specially contaminated films, where the electron–electron interaction is intensified through the occurrence of weak localization effects, T^* can reach the value of order 10 K. For temperatures $T_e > T^*$ (but $T_e < T_D$), the electron relaxation in relatively thick films does not involve direct electron–electron interaction, but occurs indirectly, through the exchange by phonons. It was shown earlier by one of the authors of Ref. [104] that the electron distribution function, resembling a Fermi one in shape, is also formed in relatively thin films (from which nonequilibrium phonons may escape to the substrate without being re-absorbed by electrons) solely as a result of phonons being emitted by 'hot' electrons. The consideration relied on a rather strong assumption that all the energy acquired from the electric field is converted to the electron temperature, which is unjustified and, as will be seen from the further analysis, does not correspond to the actual solution to the problem if the electric field strength is not very small. In both cases, the characteristic thermalization time for electrons is that of electron–phonon collisions, τ_{ep}. We also note that in optically thick films the uniformity of electron temperature over the film thickness is furnished by the fast withdrawal of electrons from the skin-layer and high electron heat conductivity compared to the phonon heat conductivity [103]. Because of an additional diffusive reduction in the density of hot electrons, the electron subsystem is thermalized substantially faster, so that for optically thick films the approximation of instantaneous thermalization leads to good agreement between theoretical and experimental results. Reference [104] dealt with the case of weak 'heating', but we, while considering the EPE, are dealing with very strong heating and need, therefore, to carry out a consistent kinetic consideration of both electron and phonon subsystems, which comprises the main content of Refs [30, 105, 106].

In the kinetic description, the behavior of electrons obeys the Boltzmann equation for the electron distribution function $f(\mathbf{r}, \mathbf{p}, t)$ with related collision integrals:

$$\frac{\partial f}{\partial t} + \mathbf{v}\frac{\partial f}{\partial \mathbf{r}} + \frac{d\mathbf{p}}{dt}\frac{\partial f}{\partial \mathbf{p}} = I_{ee} + I_{ep} + I_{ed}\,,$$

$$\frac{d\mathbf{p}}{dt} = e\left[\boldsymbol{\mathcal{E}}(\mathbf{r}, t) + \mathbf{v} \times \mathbf{B}(\mathbf{r}, t)\right],$$

where I_{ee}, I_{ep}, and I_{ed} are the respective collision integrals of electrons with electrons, electrons with phonons, and electrons with impurities and lattice defects, $\mathbf{v}$ is the velocity, $\mathbf{r}$ is the radius vector, $\mathbf{p}$ is the electron momentum, t is the time, $\mathcal{E}$ is the electric field strength, and $\mathbf{B}$ is the magnetic field induction. In what follows, we assume that the magnetic field is absent.

The phonon distribution function also obeys the kinetic equation with collision integrals, namely

$$\frac{\partial N_p(\mathbf{q}_p)}{\partial t} + \mathbf{v}_q \frac{\partial N_p(\mathbf{q}_p)}{\partial \mathbf{r}} = I_{pe} + I_{pp} + I_{pd}\,, \tag{5.4}$$

where I_{pe}, I_{pp}, and I_{pd} are the respective collision integrals of phonons with electrons, phonons with phonons, and phonons with impurities and lattice defects, $\mathbf{v}_q = \hbar\partial\Omega/\partial\mathbf{q}_p$ is the phonon speed, $\mathbf{q}_p$ is its momentum, and $N_p(\mathbf{q}_p)$ is the phonon distribution function. Recognizing that collisions of electrons with impurities, phonons, and defects lead to the isotropization of the electron distribution function, we seek it in the form

$$f(\mathbf{p},t) = f\big(E(p)\big) + \mathbf{f}_1\big(E(p)\big)\,\frac{\mathbf{p}}{p}\,. \tag{5.5}$$

Taking into account that energy transfer in collisions of electrons with phonons is very small, we simplify the electron–photon collision integrals, namely, we expand the isotropic part of the electron distribution function in series in small energy transfer, retaining the quadratic terms, viz.

$$\begin{aligned} f(\mathbf{p}\pm\mathbf{q}_p) &\equiv f\big(E(\mathbf{p})\pm\hbar\Omega(\mathbf{q}_p)\big) \\ &= f\big(E(p)\big) \pm \frac{\partial f\big(E(p)\big)}{\partial E}\,\hbar\Omega + \frac{\partial^2 f\big(E(p)\big)}{\partial E^2}\,\frac{(\hbar\Omega)^2}{2}\,, \end{aligned}$$

and substitute this expansion into the collision integrals. Let us take into account the specific form of transition probability $w(q_p)$ and also the frequency of phonon–phonon collisions $\nu_{pp}(q_p)$:

$$w(q_p) = w_0 q_p\,, \quad w_0 = \frac{4\pi^2 m^2 \varepsilon_{1A}^2}{2(2\pi\hbar)^3\rho}\,,$$

$$\nu_{pp}(q_p) = \nu_{pp0} q_p^2\,, \quad \nu_{pp0} = \frac{T_{gr}^3 c_s}{a_{gr} T_D M_c}\,,$$

where $\hbar\Omega(q_p) = c_s q_p$, ε_{1A} is the constant of the deformation potential, T_{gr} is the lattice temperature, M_c is the net mass of two atoms, c_s is the speed of sound, and a_{gr} is the lattice parameter.

The distribution functions for electrons $f(\varepsilon)$, as well as for phonons $N_p(q_p)$, are dimensionless and satisfy the following normalization conditions

$$\frac{1}{2\pi^2}\left(\frac{2m}{\hbar^2}\right)^{3/2}\int_0^\infty E^{1/2} f(E)\,\mathrm{d}E = n\,, \tag{5.6}$$

where n is the number density of electrons in the valence band (in metals it is also the conduction band, since it is only partially filled), and

$$\frac{1}{2\pi^2}\left(\frac{1}{\hbar^3}\right)\int_0^{q_D} q_p^2 N_p(q_p)\,\mathrm{d}q_p < \infty\,, \tag{5.7}$$

where q_D is the Debye phonon momentum defined by the identity $k_B T_D = c_s q_D$. Hereinafter, all quantities are listed for nickel (in which case computational and observational results can be compared [108]): $c_s = 5\times10^5$ cm s^{-1}, $T_D = 375$ K; hence, the maximum phonon momentum is 103×10^{-19} g cm s^{-1}, the electron number density in the valence band $n = 2.5\times10^{22}$ cm^{-3}, the nickel density $\rho = 8.9$ g cm^{-3}, and the lattice constant (the distance between neighboring atoms) $a = 3.5\times10^{-8}$ cm.

In a thermodynamically equilibrium state, the electron distribution function $f(E)$ is given by the Fermi–Dirac distribution

$$f(E) = \left[\exp\left(\frac{E-E_F}{k_B T_e}\right)+1\right]^{-1}, \tag{5.8}$$

where $E_F = 5\times10^{-12}$ erg, and T_e is the temperature of the electron component [in experiments, it reached 20 K and 80 K, coinciding with the lattice (phonon) temperature initially (before the electric field $\mathcal{E} = 0.31$ CGSE units $= 94$ V cm^{-1} was switched on)]. Based on the residual nickel resistivity, $\rho_{cur} = 3\times10^{-6}\ \Omega$ cm, we determine the frequency of electron collisions with impurities and lattice defects: $\nu_{ed} = 3\times10^{13}$ s^{-1}. The frequency of electron–phonon collisions depends on the phonon momentum as $\nu_{ep} = \nu_{ep0}\,q/q_D$, and $\nu_{ep0} = 2\times10^{10}$ s^{-1}. Since numerical integration of the electron–electron collision integral presents considerable difficulties due to its nonlinearity, and since its role consists in redistributing the energy supplied by the outer electric field between electrons (quasithermalization), integrating the coupled system for isotropic electron and phonon distribution functions, we limit ourselves to retaining only the electron–phonon and phonon–electron collision integrals, but on the time interval t_{ee} during which the contribution from electron–electron collisions can be omitted. The time t_{ee} is estimated by its lower bound from the condition that the energy released in the conductor upon the passage of electric current heats (it is assumed that electrons have relaxed over this time to a thermodynamically equilibrium state) the electron subsystem to a temperature comparable to the initial one, i.e., one has

$$\frac{\mathcal{E}^2}{\rho_{cur}}\,t_{ee} = c_p\,\rho\,T_e\,, \tag{5.9}$$

where $c_p = 25$ J kg^{-1} K^{-1} is the specific heat for nickel. From Eqn (5.9) we find the expression for the time interval t_{ee}:

$$t_{ee} = c_p\,\rho\,T_e\,\frac{\rho_{cur}}{\mathcal{E}^2}\,. \tag{5.10}$$

For the electric field strength $\mathcal{E} = 0.31$ CGSE units $= 94$ V cm^{-1}, the time $t_{ee} = 45\tau_{ep0}$. We will measure time in units inverse to the electron–phonon collision frequency in both equations for electron and phonon distribution functions. The energies of electrons E and phonons $c_s q_p$ are put into a dimensionless form by dividing their by $k_B T_e$. In this case, the system of equations is written out as

$$\begin{aligned} \frac{\partial f(\tilde p)}{\partial\tilde t} - \Delta\tilde\varepsilon\,\frac{1}{\tilde p^2}\,\frac{\partial}{\partial\tilde p}\left[\tilde p^2\,\frac{\partial f(\tilde p)}{\partial\tilde p}\right] &= \frac{1}{\tilde p^2} \\ &\times \frac{\partial}{\partial\tilde p}\left\{\frac{1}{\tilde p}\,\frac{\partial f(\tilde p)}{\partial\tilde p}\int_0^{2\tilde p}\mathrm{d}\tilde q_p\,\tilde q_p^4\left[N_p(\tilde q_p)+\frac12\right]\right. \\ &\left. + f(\tilde p)\big(1-f(\tilde p)\big)\sqrt{\frac{1}{\alpha}}\int_0^{2\tilde p}\mathrm{d}\tilde q_p\,\tilde q_p^3\right\}, \end{aligned} \tag{5.11}$$

$$\begin{aligned} \frac{\partial N_p(\tilde q_p)}{\partial\tilde t} &= \int_{q_p/2}^\infty \mathrm{d}\tilde p\,\tilde p\left\{\frac{1}{\alpha}\,f(\tilde p)\big(1-f(\tilde p)\big) + \big[N_p(\tilde q_p)+1-f(\tilde p)\big]\right. \\ &\left. \times\left[\frac{1}{\sqrt\alpha}\,\tilde q_p\,\frac{\partial f(\tilde p)}{\tilde p\,\partial\tilde p} + \tilde q_p^2\,\frac{\partial}{2\tilde p\,\partial\tilde p}\,\frac{\partial f(\tilde p)}{\tilde p\,\partial\tilde p}\right]\right\}, \end{aligned} \tag{5.12}$$

where

$$\tilde t = t\nu_{ep0}\,, \quad \Delta\tilde\varepsilon = \frac{e^2\mathcal{E}^2}{6m\nu_{ep0}\nu_{ed}k_B T_e}\,, \quad \tilde p = \frac{p}{\sqrt{2mk_B T_e}}\,,$$

$$\tilde q_p = \frac{q_p}{\sqrt{2mk_B T_e}}\,,$$

$$\alpha = \frac{mc_s^2}{2k_B T_e}\,, \quad 0 \leqslant \tilde q_p \leqslant 42.5\,.$$

Integration of systems (5.11) and (5.12) was carried out with the help of fully conservative difference schemes. The conservative character of the scheme is a necessary requirement, since only it ensures that errors do not accumulate in computations over long time intervals (see, for example, Ref. [107]). The essential point consists in satisfying several conservation laws; in the case considered, they are the laws of conservation of energy and particles.

5.3 Results of numerical modeling and their discussion

As a result of numerical simulations, nonstationary distribution functions for electrons $f(p)$ and phonons $N_{\rm p}(q_{\rm p})$ over momenta have been found. Figure 18 plots the dependence of the electron distribution function on dimensionless momentum at different instants of time. The leftmost curve corresponds to the thermodynamically equilibrium function, which is also the initial one for the solution of systems of equations (5.11) and (5.12). As can be seen from Fig. 18 (curves shift to the right with time), the electron distribution function deviates more and more from the equilibrium function as time progresses.

It is thus established that the energy received by the electron subsystem from the external electric field is partially transferred to the phonon subsystem as a result of electron–phonon collisions (a small portion is involved because of the quasielastic character of electron–phonon collisions); its largest part does not contribute to the formations of the thermodynamically equilibrium electron distribution function (contrary to what is frequently assumed; see, for example, Ref. [104]), but is channelled in the formation of intense high-energy tails. Such a drastic modification of the electron distribution function causes the formation of a phonon distribution function enriched very strongly by phonons with an energy close to the Debye one. Our results deviate significantly from the results of Ref. [107], where the phonon distribution function practically coincides with the Bose–Einstein distribution in this range of momenta, but possesses a temperature corresponding to that of the electron subsystem. As follows from our numerical simulations, the 'temperature' (more precisely, the mean energy of electrons, since the electron distribution function strongly departs from the thermodynamically equilibrium form) of the electron distribution function varies insignificantly, i.e., the thermalization of the energy obtained from the electric field does not happen, but high-energy tails are formed, which are responsible for this cardinal change in the phonon distribution function. High-energy tails with ever growing intensity develop with time in the phonon distribution function, because the momentum transfer in electron–photon collisions implies a rather small energy transfer; many phonons are born at the Debye energy, i.e., their distribution function is enriched with the Debye phonons. Further, we analyze the behavior of the product of the phonon distribution function and the cubed dimensionless momentum for the thermodynamically equilibrium case (Bose–Einstein distribution) and the phonon distribution function at various moments of time after the electric field starts to act (Fig. 19).

Thus, with the help of numerical modeling of the electron–phonon system in a strong pulsed electric field, which relies on fully conservative schemes, nonequilibrium distribution functions of electrons and phonons have been found, and it has been shown that:

— the isotropization of the electron distribution function occurs because of collisions with lattice defects;

— the electron distribution function does not become a thermodynamically equilibrium one because the electron–electron collisions contribute essentially less in this situation than the electron–phonon collisions, and collisions with the 'alien' subsystem do not result in thermalization;

— the distribution functions for electrons and phonons contain high-energy tails because the momentum transfer in electron–phonon collisions implies a rather small energy transfer;

— many phonons are born in the vicinity of the Debye energy, i.e., the phonon distribution function is enriched with the Debye phonons.

By way of illustration, Fig. 20a presents the dependences of the phonon distribution function multiplied by the cubed dimensionless momentum for the thermodynamically equilibrium Bose–Einstein function corresponding to the temperature of the substrate (dashed curve), the stationary phonon distribution function taken from Ref. [107] (solid curve), and the nonequilibrium phonon distribution function from Ref. [105] (the dotted curve corresponding to the time moment $t_{\rm ee} = 50\tau_{\rm ep0}$, which is a characteristic energy relaxation time due to collisions between electrons) on the

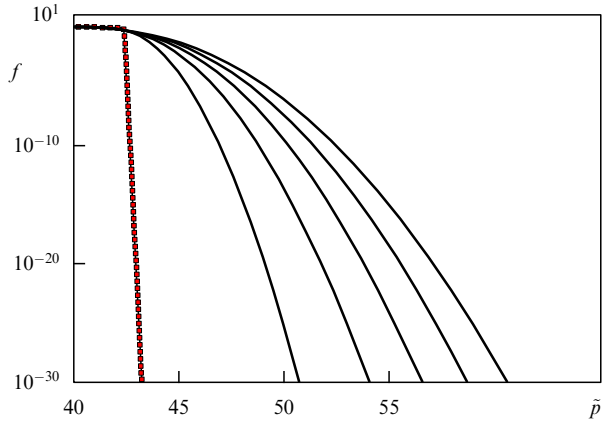

Figure 18. Dependence of the electron distribution function on the dimensionless momentum at different time moments ($t = 0$, 10, 20, 30, 40, and 50); the curves shift to the right with increasing time $\tilde{t}$.

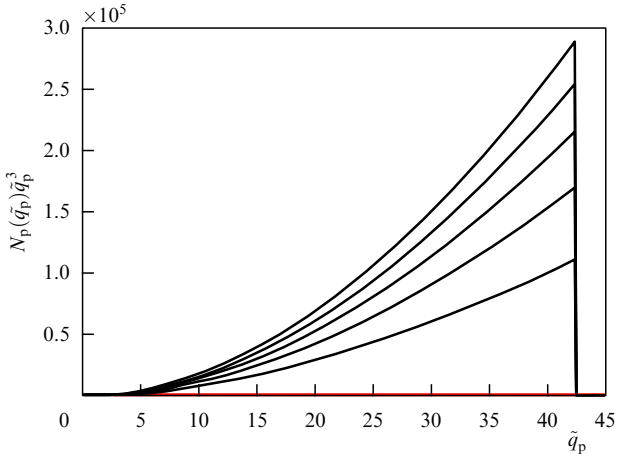

Figure 19. Dependence of the phonon distribution function multiplied by the cubed momentum (at time moments $\tilde{t} = 0$, 10, 20, 30, 40, and 50) on the dimensionless momentum; the curves go up with increasing time $\tilde{t}$.

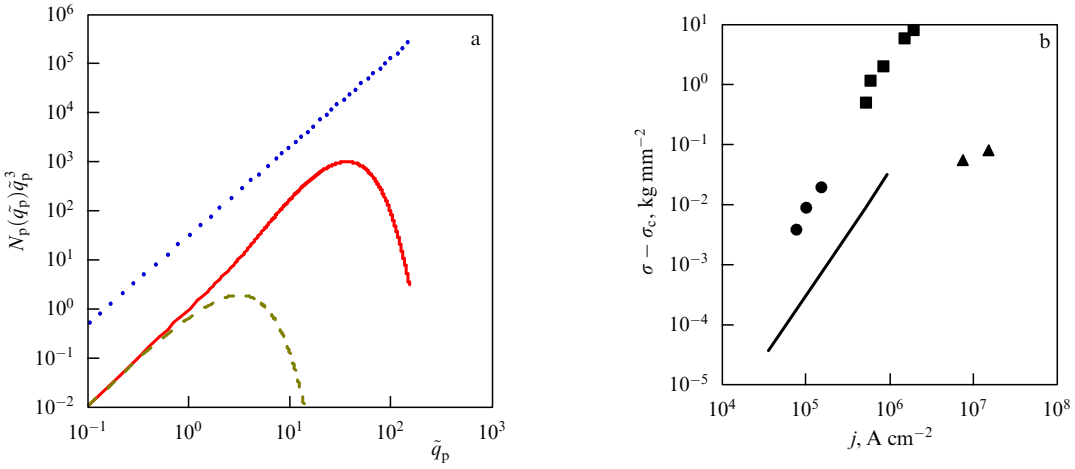

Figure 20. (a) Dependences of the phonon distribution function multiplied by the cubed dimensionless momentum for the thermodynamically equilibrium Bose–Einstein function corresponding to the temperature of the substrate (lower dashed line), the stationary phonon distribution function from Ref. [107] (solid line), and the nonequilibrium phonon distribution function from Ref. [105] (dotted curve) on the dimensionless momentum $\tilde{q}_p$ under the action of electric field $\mathcal{E} = 96$ V cm^{-1}. (b) The drop in load at constant deformation rate as a function of current density. The solid line corresponds to Joule heating; triangles correspond to theoretical nonequilibrium consideration; dots plot the data of Refs [27, 28] at $T_{start} = 78$ K, and squares plot the experimental data obtained by V P Lebedev at $T_{start} = 293$ K for a constant deformation rate of $\dot{\varepsilon}_d = 2.7 \times 10^{-4}$ s^{-1} and the following parameters $\rho_d = 10^8$ cm^{-2}, $l = 10^3 b$, $b = 3.52 \times 10^{-8}$ cm, $x_c = 2b$, $U_0 = 8 \times 10^{-13}$ erg, $L = 10^{-4}$ cm, and $\mu = 1.2 \times 10^{12}$ dyne cm^{-2}.

dimensionless momentum. The dependences are given for the following parameters: the acting electric field $\mathcal{E} = 96$ V cm^{-1}, the substrate temperature $T_b = 4.2$ K, the thickness of nickel film $d = 10^{-4}$ cm, and the electron temperature $T_e = 41.68$ K, which is established according to results of Ref. [107].

From Fig. 20, it is seen that under the action of electric field $\mathcal{E} = 96$ V cm^{-1} the curve for the product of the phonon distribution function and the cubed dimensionless momentum for the thermodynamically equilibrium Bose–Einstein function, corresponding to the temperature of the substrate, practically coincides with the result for the stationary (in partly nonequilibrium approximation) phonon distribution function from Ref. [107] for phonons with small momenta, and differs rather significantly (by almost two orders of magnitude) from the curve for phonons with large momenta. But, as indicated by Fig. 20, this does not lead to a substantial growth in the effective temperature serving actually as a quantity controling the effects of electroplastic deformation. The nonequilibrium phonon distribution function from work [105] provides the product of the distribution function and the cubed dimensionless momentum, which is more than two orders of magnitude larger than the relevant product for the partly nonequilibrium situation over the entire range of phonon momenta. The reduction in the load stress computed for the nonequilibrium case is in satisfactory agreement with experimental data.

Let us compare the reduction in the load stress as a function of the density of electric current passing through a thin metallic sample under the condition of stationary strain rate (the experimental dependence was obtained by V P Lebedev) with the theoretical prediction obtained in Section 5.3. By considering the Landau–Gofman model [108] and formulas (5.1)–(5.3), the following expression for the plastic strain rate was derived:

$$\dot{\varepsilon}_d = b\rho_d l v_0(T) \exp\left[-\frac{bL^2\sigma_c^2}{4S\mu k_B T_{eff}(T)}\left(1-\frac{\sigma}{\sigma_c}\right)^2\right].$$

Since the strain rate was stationary in the experiments, we obtain the relationship between jumps in the load and the effective temperature, the expression for which is given in Ref. [105]:

$$\delta\sigma = \sigma(j=0) - \sigma(j) = 10^{-8}\sigma_c\left[\sqrt{a(j)\,T_{eff}(j)} - \sqrt{a(0)\,T_{eff}(0)}\right],$$

$$a(0) = a(T_{start}), \quad T_{eff}(0) = T_{eff}(T_{start}), \quad \sigma_c = \frac{2}{bL}\frac{U_0}{x_c},$$

$$a(T) = \ln\left(\frac{\dot{\mathcal{E}}_0(T)}{\dot{\mathcal{E}}_d}\right)\frac{4\mu S k_B}{bL^2\sigma_c^2}, \quad \dot{\mathcal{E}}_0(T) = b\rho_d l v_0(T),$$

where $T(j)$ is expressed in terms of Joule heating in an equilibrium case or through the respective effective temperature, which is defined by the nonequilibrium phonon distribution function. Substituting the parameters corresponding to the experiment into this relationship yields the theoretical dependence plotted together with the experimental data in Fig. 20b. From the analysis carried out and Fig. 20, it can be seen that the dependence of load stress reduction on the current density under a constant strain rate, which would satisfactorily describe the experimental dependence, cannot be obtained (the difference is 2–3 orders of magnitude) either from the thermodynamically equilibrium approach or from the partly nonequilibrium approach proposed in Ref. [107]. Relatedly, a more promising framework for explaining anomalous electroplastic properties of metals and semiconductors observed experimentally involves computing a nonequilibrium phonon distribution function which is the solution to the above-considered two-component electron–phonon system of equations [105, 106].

6. Conclusions

This review discusses the current state of research pertaining to stationary and nonstationary nonequilibrium electron distributions with flux along the spectrum in solid state plasmas and their application to a new radioisotope current source design.

By analyzing the Boltzmann collision integral, it is shown that in a homogeneous and isotropic medium for a source and

sink localized in momentum space there is a local stationary nonequilibrium distribution for nonrelativistic charged particles interacting by the Coulomb law with account for static screening. This distribution corresponds to a constant energy flux I_1: $f^{(i)}(p) = A_i I_i p^{2s_i}$, $s_i = -(3D - 4/\beta + 2(i-1))/4$, where D is the space dimension, β is the power-law exponent in the particle interaction law ($\beta = 1$ for the Coulomb interaction), and $s_{i=1} = -5/4$. This stationary nonequilibrium distribution is also an exact solution of the collision integral in the Landau form. For electrons in a solid state plasma, the interaction between which is described by the screened Coulomb potential, a local nonequilibrium distribution function may form which corresponds to a constant energy flux in momentum space. Analytical consideration was performed for a stationary source and sink localized in momentum space. Numerical modeling in the framework of the Landau–Fokker–Planck collision integral with the help of fully conservative difference schemes allows one to find nonequilibrium particle distribution functions for sources and sinks which are nonlocal, nonstationary, and nonconforming in momentum space (as is the case, for example, in ionization by direct collisions and wake waves). The existence conditions and the intensity of energy flux in momentum space are found, which allow the formation of the nonequilibrium distribution function for electrons with energy exceeding the Fermi energy. It is shown how the results obtained can be used to predict the behavior of semiconductors with their intrinsic and impurity conductivities upon irradiating them by beams of fast ions or laser radiation. The existing and presented results of experimental research on energy and angular distributions of secondary emission electrons, induced by ions, including molecular ions, witness in favor of the importance of ionization by wake fields excited by ions. The experimental results are in good agreement with theoretical predictions. Based on theoretical research into nonequilibrium electron distributions induced by ion beams in a solid state plasma, a new method is proposed for transforming fission energy into electric energy. A detailed comparison of the current source based on this principle with existing ones is carried out. The advantages and disadvantages of each existing type of radioisotope current sources are considered. The advantages of the proposed source are described and how to implement it is outlined.

The mechanism of the EPE in the framework of the model of a dislocation string passing stoppers as a result of its excitation by phonons is studied and substantiated. With the aid of numerical modeling of an electron–phonon system placed in a strong pulsed electric field, relying on fully conservative schemes, nonequilibrium distribution functions are found for electrons and phonons, and it is shown that the electron and phonon distribution functions exhibit high-energy tails, i.e., many phonons are born in the vicinity of the Debye energy and the distribution function is enriched with Debye phonons.

Based on the random impact model (in the framework of the Langevin approach), which is due to phonons in our problem, it is demonstrated that

— the thermodynamic approach cannot describe the electroplastic deformation effect;

— based on the actual phonon distribution function found as the solution of the two-component electron–phonon system of equations for the case involving the action of a strong impulse electric field on a metal, it is possible to explain anomalous electroplastic properties of metals and semiconductors observed experimentally, i.e., the EPE.

The authors regret that, because of limitations on the review size, they had to omit certain interesting and important results. To partly compensate for this gap, the list of references includes several reviews [109–114].

References

1. Kolmogoroff A N *C. R.* (*Dokl.*) *Acad. Sci. USSR* **30** 301 (1941) [*Dokl. Akad. Nauk SSSR* **30** 299 (1941)]
2. Zakharov V E *J. Appl. Mech. Tech. Phys.* **6** (4) 22 (1965) [*Zh. Prikl. Mekh. Tekh. Fiz.* (4) 35 (1965)]
3. Silin V P *Vvedenie v Kineticheskuyu Teoriyu Gazov* (Introduction into the Kinetic Gas Theory) (Moscow: Nauka, 1971)
4. Rosenbluth M N, MacDonald W M, Judd D L *Phys. Rev.* **107** 1 (1957)
5. Trubnikov B A, in *Reviews of Plasma Physics* Vol. 1 (Ed. M A Leontovich) (New York: Consultants Bureau, 1965) p. 105 [Translated from Russian: *Voprosy Teorii Plazmy* (Problems in the Plasma Theory) Issue 1 (Ed. M A Leontovich) (Moscow: Gosatomizdat, 1963) p. 98]
6. Gurov K P *Osnovaniya Kineticheskoi Teorii*: *Method N N Bogolyubova* (Foundations of Kinetic Theory: N N Bogoliubov Method) (Moscow: Nauka, 1966)
7. Gurov K P, in *Nonequilibrium Phenomena I*: *the Boltzmann Equation* (Eds J L Leibowitz, E W Montroll) (Amsterdam: North-Holland, 1983) [Translated into Russian (Moscow: Mir, 1986)]
8. Chapman S, Cowling T G *The Mathematical Theory of Non-uniform Gases; An Account of the Kinetic Theory of Viscosity, Thermal Conduction, and Diffusion in Gases* (Cambridge: Univ. Press, 1952) [Translated into Russian (Moscow: IL, 1960)]
9. Akhiezer A I, Pomeranchuk I Ya *Nekotorye Voprosy Teorii Yadra* (Some Questions from the Theory of Nucleus) (Moscow – Leningrad: Gostekhizdat, 1948)
10. Kats A V et al., Preprint No. 42 (Khar'kov: Inst. of Radiophysics and Electronics, Acad. of Sci. of Ukrainian SSR, 1974)
11. Kats A V et al. *JETP Lett.* **21** 5 (1975) [*Pis'ma Zh. Eksp. Teor. Fiz.* **21** 13 (1975)]
12. Karas' V I *Sov. Tech. Phys. Lett.* **1** 438 (1975) [*Pis'ma Zh. Tekh. Fiz.* **1** 1020 (1975)]
13. Karas' V I, Moiseev S S, Novikov V E *Sov. Phys. JETP* **44** 744 (1976) [*Zh. Eksp. Teor. Fiz.* **71** 1421 (1976)]
14. Gradshteyn I S, Ryzhik I M *Tables of Integrals, Series, and Products* (New York: Academic Press, 1980) [Translated from Russian: *Tablitsy Integralov, Summ, Ryadov i Proizvedenii* (Moscow: Nauka, 1971)]
15. Kats A V et al. *Sov. Phys. JETP* **44** 93 (1976) [*Zh. Eksp. Teor. Fiz.* **71** 177 (1976)]
16. Karas' V I, Abstract of Doct. Phys. Math. Sci. Thesis (Kharkov: Gorky Kharkov State Univ., 1988)
17. Karas' V I, Moiseev S S, Shuklin A P *Ukr. Fiz. Zh.* **25** 820 (1980)
18. Samarskii A A *The Theory of Difference Schemes* (New York: Marcel Dekker, 2001) [Translated from Russian: *Teoriya Raznostnykh Skhem* (Moscow: Nauka, 1977)]
19. Samarskii A A, Popov Yu P *Raznostnye Skhemy Gazovoi Dinamiki* (The Difference Schemes of Gas Dynamics) (Moscow: Nauka, 1975)
20. Bobylev A V *Sov. Sci. Rev. Sect. C Math. Phys. Rev.* **7** 111 (1988)
21. Bobylev A V, Chuyanov V A *USSR Comput. Math. Math. Phys.* **16** (2) 121 (1976) [*Zh. Vychisl. Mat. Mat. Fiz.* **16** 407 (1976)]
22. Potapenko I F, Chuyanov V A *USSR Comput. Math. Math. Phys.* **19** (2) 192 (1979) [*Zh. Vychisl. Mat. Mat. Fiz.* **19** 458 (1979)]
23. Potapenko I F, Chuyanov V A *USSR Comput. Math. Math. Phys.* **20** (2) 249 (1980) [*Zh. Vychisl. Mat. Mat. Fiz.* **20** 513 (1980)]
24. Bobylev A V, Potapenko I F, Chuyanov V A *USSR Comput. Math. Math. Phys.* **20** (4) 190 (1980) [*Zh. Vychisl. Mat. Mat. Fiz.* **20** 993 (1980)]
25. Bobylev A V, Potapenko I F, Chuyanov V A *Sov. Phys. Dokl.* **25** 994 (1980) [*Dokl. Akad. Nauk SSSR* **255** 1348 (1980)]
26. Potapenko I F, Chuyanov V A *USSR Comput. Math. Math. Phys.* **22** (3) 269 (1982) [*Zh. Vychisl. Mat. Mat. Fiz.* **22** 751 (1982)]
27. Potapenko I F et al. *Phys. Rev. E* **56** 7159 (1997)

28. Potapenko I F, de Azevedo C A *J. Comput. Appl. Math.* **103** 115 (1999)
29. Karas' V I, Potapenko I F *Plasma Phys. Rep.* **28** 837 (2002) [*Fiz. Plazmy* **28** 908 (2002)]
30. Karas' V I, Potapenko I F *Comput. Math. Math. Phys.* **46** (2) 294 (2006) [*Zh. Vychisl. Mat. Mat. Fiz.* **46** (2) 307 (2006)]
31. Potapenko I F, Bornatici M, Karas V I *J. Plasma Phys.* **71** 859 (2005)
32. Kononenko S I et al. *Plasma Phys. Rep.* **30** 761 (2004) [*Fiz. Plazmy* **30** 722 (2004)]
33. Gurzhi R N *Sov. Phys. JETP* **6** 506 (1958) [*Zh. Eksp. Teor. Fiz.* **35** 965 (1958)]
34. Ziman J M *Electrons and Phonons* (Oxford: Clarendon Press, 1960) [Translated into Russian (Moscow: IL, 1962)]
35. Basko M M, Sokolovskii M V, Preprint No. 177 (Moscow: ITEP, 1980)
36. Kalashnikov N P, Remizovich V S, Ryazanov M I *Collisions of Fast Charged Particles in Solids* (New York: Gordon and Breach, 1985) [Translated from Russian: *Stolknoveniya Bystrykh Zaryazhennykh Chastits v Tverdykh Telakh* (Moscow: Atomizdat, 1980)]
37. Otsuki Y-H *Charged Beam Interactions with Solids* (New York: Taylor and Francis, 1983) [Translated into Russian (Moscow: Mir, 1985)]
38. Karas' V I, Moiseev S S, Novikov V E *JETP Lett.* **21** 245 (1975) [*Pis'ma Zh. Eksp. Teor. Fiz.* **21** 525 (1975)]
39. Hansen L K (Ed.) *Thermionic Converters and Low-Temperature Plasma* (Oak Ridge, TN: Technical Information Center, U.S. Dept. of Energy, 1978); Moizhes B Ya, Pikus G E (Eds) *Termoemissionnye Preobrazovateli i Nizkotemperaturnaya Plazma* (Moscow: Nauka, 1973)
40. Aseevskaya A S, Ivkin E B, Kolomiets B G *Sov. Tech. Phys. Lett.* **2** 117 (1976) [*Pis'ma Zh. Tekh. Fiz.* **2** 305 (1976)]
41. Knecht W L *Appl. Phys. Lett.* **6** 99 (1965)
42. Knecht W L *Appl. Phys. Lett.* **8** 254 (1966)
43. Anisimov S I et al. *Deistvie Izlucheniya Bol'shoi Moshchnosti na Metally* (The Action of High-Power Radiation on Metals) (Eds A M Bonch-Bruevich, M A El'yashevich) (Moscow: Nauka, 1970)
44. Anisimov S I, Ivanov M F *Sov. Phys. Dokl.* **20** 758 (1975) [*Dokl. Akad. Nauk SSSR* **225** 280 (1975)]
45. Parilis E S, Kishinevskii L M *Sov. Phys. Solid State* **3** 885 (1961) [*Fiz. Tverd. Tela* **3** 1219 (1961)]
46. Sternglass E J *Phys. Rev.* **108** 1 (1957)
47. Kaminsky M *Atomic and Ionic Impact Phenomena on Metal Surfaces* (New York: Academic Press, 1965) [Translated into Russian (Moscow: Mir, 1967)]
48. Arifov U A *Interaction of Atomic Particles with a Solid Surface* (New York: Consultants Bureau, 1969) [Translated from Russian: *Vzaimodeistvie Atomnykh Chastits s Poverkhnost'yu Tverdogo Tela* (Moscow: Nauka, 1968)]
49. Medved D B, Strausser Y E *Adv. Electron. Electron. Phys.* **21** 101 (1965) [Abridged Russian Translation: *Usp. Fiz. Nauk* **91** 485 (1967)]
50. Frischkorn H J et al. *Nucl. Instrum. Meth. Phys. Res.* **214** 123 (1983)
51. Petrov N N, Abroyan I A *Diagnostika Poverkhnosti s Pomoshch'yu Elektronnykh Puchkov* (Surface Diagnostics with the Help of Ion Beams) (Leningrad: Izd. LGU, 1977)
52. Abroyan I A, Eremeev M A, Petrov N N *Sov. Phys. Usp.* **10** 332 (1967) [*Usp. Fiz. Nauk* **92** 105 (1967)]
53. Dorozhkin A A, Petrov N N, Petrov A A *Izv. Akad. Nauk SSSR Ser. Fiz.* **40** 1687 (1976)
54. Mechbach W, Braunstein G, Arista N *J. Phys. B At. Mol. Phys.* **8** L344 (1975)
55. Hasselkamp D, Scharmann A *Surf. Sci.* **119** L388 (1982)
56. Hasselkamp D, Scharmann A *Phys. Lett. A* **96** 259 (1983)
57. Hasselkamp D, Hippler S, Scharmann A *Nucl. Instrum. Meth. Phys. Res. B* **2** 475 (1984)
58. Krebs K H *Vacuum* **33** 555 (1983)
59. Hasselkamp D et al. *Nucl. Instrum. Meth.* **180** 349 (1981)
60. Baragiola R A, Alonso E V, Oliva Florio A *Phys. Rev. B* **19** 121 (1979)
61. Alonso E V et al. *Phys. Rev. B* **22** 80 (1980)
62. Hasselkamp D, Scharmann A *Phys. Status Solidi A* **79** K197 (1983)
63. Holmén G, Svensson B, Burén A *Nucl. Instrum. Meth. Phys. Res.* **185** 523 (1981)
64. Koyama A, Yagi E, Sakairi H *Jpn. J. Appl. Phys.* **15** 1811 (1976)
65. Koyama A, Shikata T, Sakairi H *Jpn. J. Appl. Phys.* **20** 65 (1981)
66. Mironov E S, Nemenov L M *Sov. Phys. JETP* **5** 188 (1957) [*Zh. Eksp. Teor. Fiz.* **32** 269 (1957)]
67. Svensson B, Holmén G *Phys. Rev. B* **25** 3056 (1982)
68. Frischkorn H J et al. *Phys. Rev. Lett.* **49** 1671 (1982)
69. Sternglass E J *Phys. Rev.* **95** 345 (1954)
70. Garnir H P, Dumont P D, Baudinet-Robinet Y *Nucl. Instrum. Meth. Phys. Res.* **202** 187 (1982)
71. Rothard H et al. *Phys. Rev. A* **51** 3066 (1995)
72. Mischler J et al. *Surf. Sci.* **136** 532 (1984)
73. Anno J N *J. Appl. Phys.* **34** 3495 (1963)
74. Koyama A et al. *Jpn. J. Appl. Phys.* **21** 1216 (1982)
75. Svensson B, Holmén G *J. Appl. Phys.* **52** 6928 (1981)
76. Schou J *Phys. Rev. B* **22** 2141 (1980)
77. Batrakin E N et al. *Poverkhnost'* (12) 82 (1986)
78. Batrakin E N et al. *Sov. Phys. JETP* **62** 633 (1985) [*Zh. Eksp. Teor. Fiz.* **89** 1098 (1985)]
79. Babenko V A et al. *Sov. Phys. Tech. Phys.* **25** 508 (1980) [*Zh. Tekh. Fiz.* **50** 848 (1980)]
80. Gott Yu V *Vzaimodeistvie Chastits s Veshchestvom v Plazmennykh Issledovaniyakh* (Interaction of Particles with Matter in Plasma Research) (Moscow: Atomizdat, 1978)
81. Agranovich V M et al. *Sov. Phys. JETP* **30** 220 (1970) [*Zh. Eksp. Teor. Fiz.* **57** 401 (1969)]
82. Agranovich V M et al. *Sov. Phys. JETP* **34** 805 (1972) [*Zh. Eksp. Teor. Fiz.* **61** 1511 (1971)]
83. Daukeev D K, Lebedev S Ya *Sov. Phys. Solid State* **12** 507 (1970) [*Fiz. Tverd. Tela* **12** 655 (1970)]
84. Baragiola R A, Dukes C A, Riccardi P *Nucl. Instrum. Meth. Phys. Res. B* **182** 73 (2001)
85. Bronshtein I M, Fraiman B S *Vtorichnaya Elektronnaya Emissiya* (Secondary Electron Emission) (Moscow: Nauka, 1969)
86. Siegbahn K (Ed.) *Alpha- Beta- and Gamma-Ray Spectroscopy* Vol. 1 (Amsterdam: North-Holland Publ. Co., 1965) [Translated into Russian (Moscow: Atomizdat, 1969)]
87. Price W J *Nuclear Radiation Detection* (New York: McGraw-Hill, 1958) [Translated into Russian (Moscow: IL, 1960)]
88. Kononenko S I *Dopovidi Nats. Akad. Nauk Ukrainy* (1) 87 (2001)
89. Soboleva N A, Melamid A E *Fotoelektronnye Pribory* (Photoelectron Instruments) (Moscow: Vysshaya Shkola, 1974)
90. Fomenko V S, Podchernyaeva I A *Emissionnye i Absorbtsionnye Svoistva Veshchestv i Materialov* (Emission and Absorption Properties of Matter and Materials) (Moscow: Atomizdat, 1975)
91. Rosebury F *Handbook of Electron Tube and Vacuum Techniques* (Reading, Mass.: Addison-Wesley, 1965) [Translated into Russian (Moscow: Energiya, 1972)]
92. Zhurenko V P et al. *Plasma Phys. Rep.* **29** 130 (2003) [*Fiz. Plazmy* **29** 150 (2003)]
93. Karas' V I, Moiseev S S, Preprint No. 77-24 (Kharkov: Kharkov Inst. of Physics and Technology, Acad. Sci. of the Ukrainian SSR, 1977)
94. Karas' V I, Moiseev S S *Ukr. Fiz. Zh.* **24** 1724 (1979)
95. Balebanov V M et al. *Plasma Phys. Rep.* **24** 732 (1998) [*Fiz. Plazmy* **24** 789 (1998)]
96. Balebanov V M et al. *Atomic Energy* **84** 324 (1998) [*Atom. Energ.* **84** 398 (1998)]
97. Balebanov V M et al., Author's Certificate No. 1737559; *Byull. Izobret.* (20) (1992)
98. Balebanov V M et al., Patent RF No. 2050626; *Byull. Izobret.* (35) (1995)
99. Balebanov V M et al., Patent RF No. 2054742; *Byull. Izobret.* (5) (1995)
100. Balebanov V M et al., Patent RF No. 2050625; *Byull. Izobret.* (35) (1995)
101. Gromov V E, Tsellermaier B Ya, Bazaikin V I *Elektrostimulirovannoe Volochenie: Analiz Protsessa i Mikrostruktura* (Electrosimulated Drawing: the Process Analysis and Microstructure) (Moscow: Nedra, 1996)
102. Spitsyn V I, Troitskii O A *Metallofizika* **51** 18 (1974)
103. Kosevich A M *Teoriya Kristallicheskoi Reshetki* (*Fizicheskaya Mekhanika Kristallov*) (The Theory of Crystal Lattice (Physical

Mechanics of Crystals Ser.)) (Kharkov: Vishcha Shkola, Izd. pri Khark. Gos. Univ., 1988)
104. Bezuglyi A I, Shklovskii V A *JETP* **84** 1149 (1997) [*Zh. Eksp. Teor. Fiz.* **111** 2106 (1997)]
105. Karas' V I, Potapenko I F *Vopr. Atom. Nauki Tekh. Ser. Fiz. Radiats. Povrezhd. Radiats. Mater.* (4 – 2) 42 (2009)
106. Zakharov V E, Karas' V I *Vopr. Atom. Nauki Tekh. Ser. Yad.-Fiz. Issled.* (2(66)) 204 (2010)
107. Perrin N, Budd H *Phys. Rev. Lett.* **28** 1701 (1972)
108. Landau A I, Gofman Yu I *Sov. Phys. Solid State* **16** 2220 (1975) [*Fiz. Tverd. Tela* **16** 3427 (1974)]
109. Zakharov V, Dias F, Pushkarev A *Phys. Rep.* **398** 1 (2004)
110. Zakharov V E (Ed.) *Nonlinear Waves and Weak Turbulence* (American Mathematical Society Translations, Ser. 2, Vol. 182) (Providence, RI: American Mathematical Society, 1998)
111. Musher S L, Rubenchik A M, Zakharov V E *Phys. Rep.* **252** 177 (1995)
112. Zakharov V E, L'vov V S, Falkovich G *Kolmogorov Spectra of Turbulence I. Wave Turbulence* (Berlin: Springer-Verlag, 1992)
113. Zakharov V E, in *Basic Plasma Physics* Vol. 2 (Handbook of Plasma Physics, Vol. 2, Eds A A Galeev, R N Sudan) (Amsterdam: North-Holland, 1984) p. 3 [Translated into Russian (Moscow: Energo-atomizdat, 1984) p. 48]
114. Kontorovich V M *Radiofiz. Radioastron.* **11** (1) 5 (2006)